Linear, trigonometric and hyperbolic profiles of thermal effusivity in the Liouville space and related quadrupoles: Simple analytical tools for modeling graded layers and multilayers

Jean-Claude Krapez

Linear, trigonometric and hyperbolic profiles of thermal effusivity in the Liouville space and related quadrupoles: simple analytical tools for modeling graded layers and multilayers

J.-C. Krapez[a]*

[a] *ONERA, The French Aerospace Lab, DOTA, F-13661 Salon de Provence (France).*

* (E-mail address: jean-claude.krapez@onera.fr, Telephone number: (+33) 4 90 17 01 17, Fax number: (+33) 4 90 17 01 09)

*Corresponding Author: krapez@onera.fr

Abstract –
This paper presents a series of new high-level analytical tools for the modeling of one-dimensional, transient or periodic, heat transfer in media presenting graded thermal properties (conductivity and/or specific heat), possibly in a layered configuration. They capitalize on a recent work on sequences of analytically solvable profiles and the related exact temperature solutions. These profiles describe the square root of thermal effusivity or its inverse; the independent variable is the square root of the integrated diffusion time along the considered path, as obtained after a Liouville transformation. The profiles addressed here are linear, hyperbolic or trigonometric functions of this variable. A systematic presentation is given on how to build these profiles in both partner forms, on the so-called Liouville inverse transformation to step back into the physical-depth space, and on the three quadrupole formulations. As compared to other graded profiles from the literature, the three transfer matrices are very easy to compute (only elementary functions are involved). The quadrupole approach is particularly suitable for modeling multilayers. We apply it to calculate the thermal response of a two-layer system with a graded coating of one or other of the three classes. The modulated and the transient regime have been considered. The ease of obtaining these results indicates that, upon proper arrangement, these three classes of solvable profiles may be used to compute the thermal response of continuously (or piece-wise continuously) heterogeneous media of arbitrary complexity (e.g., functionally graded materials). This also paves the way to new methods for photothermal inversion. Other research fields could benefit from these tools insofar as the evolution equation governing the observed phenomena involves variable coefficients (e.g., advection-diffusion equation, wave equation, etc.).

Keywords: Heterogeneous, Coating, Functionally graded material, Effusivity profile, Liouville transformation, Photothermal.

Nomenclature

A, B, C, D	Quadrupole entries	
A_B, A_D	Constant coefficients related to $B(\xi), D(\xi)$	
A_K, A_P	Constant coefficients related to $K(\xi, p), P(\xi, p)$	
a	Thermal diffusivity	$m^2.s^{-1}$
b	Thermal effusivity	$W.s^{1/2}.m^{-2}.K^{-1}$
$B(\xi), D(\xi)$	LIS defining the profile $s(\xi)$	-
c	Volumetric heat capacity	$W.s.m^{-3}.K^{-1}$
$C^{(\beta)}$	Function $\cosh\left(\sqrt{p+\beta}\xi\right)$	-
f	Frequency	s^{-1}
h	Heat transfer coefficient	$W.m^{-2}.K^{-1}$
$K(\xi, p)$, $P(\xi, p)$	LIS defining the thermal field $\psi(\xi, p)$	-

p	Laplace variable or Fourier variable	s^{-1} or $s^{-1}.rad$
q,r	Constant parameters	-
$s(\xi)$	Metaproperty representing either $b^{1/2}(\xi)$ or $b^{-1/2}(\xi)$	
$S^{(\beta)}$	Function $\sinh\left(\sqrt{p+\beta}\xi\right)$	-
t	Time	s
T	Temperature	K
V	"Potential" function	s^{-1}
$W(f,g)$	Wronskian of f and g	
z	Depth coordinate	m
Z	Impedance	$W^{-1}.m^2.K$
β	Coefficient (constant value of potential V)	s^{-1}
φ	Heat flux density	$W.m^{-2}$
ϕ	Laplace/Fourier transform of the heat flux density	$W.s.m^{-2}(.rad)$
λ	Thermal conductivity	$W.m^{-1}.K^{-1}$
θ	Laplace/Fourier transform of temperature	s.K(.rad)
ξ	Square root of diffusion time (SRDT)	$s^{1/2}$
ξ_c	Characteristic SRDT of the profile element	$s^{1/2}$
ψ	Liouvillian "transformed" temperature or heat flux density	
χ	Normalized logarithmic derivative of $s(\xi)$	
ω	Angular frequency	$rad.s^{-1}$

Symbols

$\hat{\xi}$	Modified SRDT	-
f', f''	Primes denote derivatives with respect to ξ	

Subscript

i	Left (i =0) or right (i =1) layer boundary	

c	Characteristic (depth or SRDT) of the profile element

Operators

$\propto$	$h \propto [f \quad g]$ means h is a LC of f and g

Abbreviations

BC	Boundary Condition
LC	Linear Combination
LF	Laplace-Fourier
LIS	Linearly independent solutions
PROFIDT	Joint Property & Field Darboux Transformation
SRDT	Square Root of Diffusion Time
VHC	Volumetric heat capacity
$\langle T \rangle$, $\langle \varphi \rangle$	With reference to the heat equations expressed in temperature or in heat flux

1. Introduction

Analytical modeling of the dynamic thermal response of materials with gradation of thermal properties in the direction perpendicular to the surface is of interest in various fields. This is an essential step in the design and optimization of the structure of functionally graded materials, such as those intended to withstand high thermal loads (e.g., thermal barriers) [1], [2], [3]. This may also be useful for interpreting the thermal response of functionally graded materials designed for other purposes, such as achieving a specific mechanical property (e.g., hardness). More specifically, it may happen that the mechanical property gradient is correlated with a thermal-property gradient, thus opening the possibility of performing an indirect evaluation of the first through a non-destructive evaluation of the latter, for example with a photothermal method (see, e.g., [4]-[15]). The thermal characterization of living biological systems, tissue engineering and biotechnology in medicine are other areas where advances in thermal modeling in complex media (namely graded media) provide indisputable benefits [16]-[19].

Analytical methods for thermal diffusion problems are restricted to objects with simple geometry and boundary conditions. In more complex situations, e.g. complicated shape, presence of inclusions, fracture or holes, complex boundary conditions or complex distribution of thermal loads, the use of numerical methods is necessary. A large number of numerical methods have been developed to solve the problem of heat diffusion in graded media: the boundary element method [20], meshfree methods like the method of fundamental solutions [21]-[23], the finite element method and its non-remeshing version, e.g. the extended finite element method [24] and the version based on extended isogeometric analysis [25]. Nevertheless, although numerical methods are capable of solving complex problems, the obtained solutions correspond to one specific case and generalization is not easy. On the opposite, in their domain of applicability, the analytical solutions are faster, more insightful, they are easy to parameterize and thus open a clearer way to a sensitivity analysis. In addition, numerical methods require some expertise in the discretization/meshing phase, which is absent from analytical methods. Because of this additional complexity, analytical methods are favored in the early stages of design or analysis. The tradeoffs between different design parameters are then easier to analyze. In a sense, analytical methods are less accurate because of the simplifying assumptions required. On the other hand, in the frame of these hypotheses, they are exact, contrary to numerical methods which always suffer from discretization errors. This is the reason for striving to widen as much as possible the scope of analytical methods. With this in mind, the purpose of present paper is to describe a new method for one-dimensional thermal modeling in graded layers or multilayers.

There is no closed-form solution for the dynamic temperature in the case of arbitrary spatial distributions of the thermal properties (basically, conductivity and the volumetric heat capacity (VHC)), even in the simplified case of one-dimensional linear transfer. This applies to both time-space and the Laplace-Fourier (LF) space. Series solutions have been proposed in time-space by implementing either the Generalized Integral Transform Technique [19], [26]-[28], radial basis functions [21]-[23] or the Spectral Parameter Power Series method [29]. However, the series must be truncated, which makes the methods approximate in essence. In addition, it is not easy to guess which set of property profiles truly corresponds to the inferred temperature solution obtained after truncation (if such a set ever exists). Moreover, steep property profiles are expected to require longer series to achieve a given accuracy.

Until recently, exact, analytical and closed-form solutions to the heat equation in the LF space were known only for a limited number of profile configurations (in time-space, their number is still lower). A profile configuration is typically defined by a set of *two* functions of depth z describing the profiles of two among the following *four* thermal properties: conductivity $\lambda(z)$, VHC $c(z)$, diffusivity $a(z)=\lambda(z)/c(z)$ and effusivity $b(z)=\sqrt{\lambda(z)c(z)}$. The profiles constituting these particular configurations will be called "solvable profiles", keeping in mind that in the z-space these solvable profiles go in pairs. For example, linear and power-law functions of z for conductivity $\lambda(z)$ and VHC $c(z)$ are solvable profiles [30]. The corresponding temperature solution in the LF space involves the modified Bessel functions of order $\nu=(1-n)/(m-n+2)$, where n and m are, respectively, the powers of depth describing conductivity and VHC [30], [31], [32] (Ref. [33] considered the case in which $m=0$). In particular, the solution related to a linear conductivity profile involves the Bessel functions of order 0; this "linear" model has been used in Refs. [4], [13], [32]-[39]. Another specific case is when conductivity is constant and VHC is a linear function of position; the temperature is then expressed in terms of Airy functions [40]. Only for a few

particular cases, i.e., when $\nu = j + 1/2,\ j = 0,\pm1,\pm2\ldots$, the temperature expression in LF space reduces to elementary functions (exponential and algebraic functions). Among them are the profiles $\lambda(z) \propto z^{2j}$ (with otherwise constant diffusivity) and the profiles $\lambda(z) \propto z^{4j/(2j-1)}$ (with otherwise constant VHC), which lead to the limiting profile $\lambda(z) \propto z^2$ for $j \to \pm\infty$. In the latter case, which corresponds to a linear profile of effusivity in z-space, the solutions in LF space can be expressed as a linear combination of power functions of the effusivity profile itself [6], [30], [33] (alternative representations are given in Refs. [34] and [41]). All previous considerations were about power-law functions of the Cartesian coordinate z. In the case of functionally-graded thick hollow cylinders, the temperature solution involves Bessel functions of order $\nu = n/(n-m-2)$ [42].

Notice that in another context, namely turbulent diffusion in the atmospheric boundary layer, the corresponding advection-diffusion equation takes the same form as the heat equation, where conductivity is replaced by the eddy diffusivity and heat capacity is replaced by the wind velocity (both parameters depend on the height above the ground surface). Linear and power-law functions were considered a long time ago to represent the height-dependency of these parameters [43]-[48]. It appears that in the simple configuration of a point load at the bottom of a semi-infinite layer, the downwind response (in the space domain, not in the LF domain) is expressible in a simple way with power and exponential functions.

When $\lambda^{1/2}(z)$ is expressed as a linear combination of trigonometric functions of $\beta_\lambda z$ or exponential functions of $\pm\beta_\lambda z$ (with otherwise constant diffusivity), where β_λ is a constant parameter, the temperature solution in the time domain is obtained by multiplying the classical solution for a homogeneous material with constant diffusivity a_0, respectively, by $\lambda^{-1/2}(z)\exp\left(\beta_\lambda{}^2 a_0 t\right)$, or by $\lambda^{-1/2}(z)\exp\left(-\beta_\lambda{}^2 a_0 t\right)$ [20].

Exponential profiles in $\beta_\lambda z$ for $\lambda(z)$ and in $\beta_c z$ for $c(z)$ have been considered in [32], [39]. The temperature solution involves Kelvin functions of order $\nu = \beta_\lambda/(\beta_\lambda - \beta_c)$; they reduce to exponential and algebraic functions when $\nu = j + 1/2,\ j = 0,\pm1,\pm2\ldots$, [32] in particular when $\beta_\lambda = 3\beta_c$ [32], [39]. When $\beta_c = 0$ we obtain Bessel functions of order 1 [32]-[34], [49], [50]. On the other side, temperature is found in terms of the hypergeometric function when a constant term is added to the exponential profile of conductivity, whereas VHC remains constant [13]. The case of arbitrary values of the constants β_λ and β_c has been solved in the time domain by the separation-of-variables method and the variable substitution method for all three geometries (plate, cylinder and sphere) [51].

Transforming the independent variable z into another variable ξ that integrates a specific aspect of the heterogeneous character of the material may offer additional possibilities in the quest for solvable profiles. A first example involves the square root of the diffusion time (SRDT), which is defined according to:

$$\xi \equiv \int^z a^{-1/2}(u)\,du \tag{1}$$

This is an essential ingredient of the Liouville transformation, which will be discussed in more detail next in the paper. Exponential functions of the SRDT ξ constitute solvable profiles for effusivity, as was shown in [52], [53]. The inferred temperature solution is expressed in terms of exponential functions in ξ.

Another example involves the integrated thermal resistance, which is defined according to:

$$\xi \equiv \int^z \lambda^{-1}(u)\,du \tag{2}$$

The power functions of ξ are solvable profiles for effusivity [54]. The general solution for temperature is a combination of Bessel functions. It reduces to elementary functions when the power m is of the form $m = -2j/(2j+1),\ k \in Z$.

Notice that once the general solution for a particular solvable profile has been obtained, it is easy to calculate the quadrupole matrix corresponding to a graded layer showing this profile. A quadrupole matrix (also called "analytical transfer matrix") provides a linear relation between the temperature/flux vectors $[\theta \quad \phi]^t$ on both sides of a layer [30], [55]. When multiple layers are joined together, the quadrupole matrix obtained by multiplying the individual matrices then relates the $[\theta \quad \phi]^t$ vectors on both sides of the multilayer slab. Finally, expressing the boundary conditions applied to the outer surfaces of the multilayer provides closure

to the problem. The quadrupole method can also be used in the presence of internal heat sources, either localized or distributed, in which case different strategies have been proposed to obtain stable solutions [56].
The quadrupole matrices for linear and exponential profiles of conductivity (with otherwise constant heat capacity) were described in Ref. [33]. A stacking of quadrupoles related to linear profiles has been considered in Ref. [38] for modeling the photothermal response of a piecewise linear depth profile of conductivity. A higher-order representation is thereby achieved, as compared with the classical piecewise constant depth profile approach. The interest of the latter is in its simplicity; it nevertheless requires subdividing the slab under study into a large number of layers (and then calculating a respectively large number of quadrupoles) if the profile aimed to be modeled presents rapid variations (see, e.g., [11], [57]). The same accuracy, however with fewer quadrupoles, would be obtained by considering linear-profile quadrupoles. Quadrupoles of even higher order could be considered; this paper fits into this perspective.
A recently described method allows infinite sequences of solvable profiles to be built together with the temperature solutions in the LF space [58]. The first operation is a Liouville transformation, which allows the heat equation to be transformed into a stationary Schrödinger equation, where the potential $V(\xi)$ depends only on $b(\xi)$, i.e., the effusivity profile vs. the SRDT ξ defined in Eq. (1). A constant potential $V(\xi)$ then gives rise to a set of solutions that were called "fundamental solutions". They are related to three classes of effusivity profiles, defined in such a way that $b^{1/2}(\xi)$, or its inverse, is a linear function of ξ, or a combination of trigonometric or hyperbolic functions of an argument proportional to the SRDT ξ. Successive Darboux transformations were then applied to both the (transformed) temperature equation and the effusivity equation (PROFIDT method - Property and Field Darboux Transformation). They provide simultaneously new solvable profiles of effusivity and the corresponding temperature solutions. Applying the PROFIDT method recursively progressively provides more sophisticated effusivity profiles, with a chance of coming close to a pre-determined profile and, hence, being able to solve the thermal problem for that specific profile with an arbitrarily small approximation error. In addition, the use of the "fundamental solutions" as seed solutions for starting the PROFIDT sequence offers the advantage that all subsequent solutions are exclusively based on *elementary functions*. A class of monotonic profiles that are particularly suitable to model semi-infinite layers, the so-called $\tanh^{\pm 1}(\hat{\xi})$-type profiles, has been described in [58] and [59]. The $\mathrm{sech}(\hat{\xi})$-type profiles are, in turn, highly flexible profiles depending on four adjustable parameters; they constitute the building blocks of what has been dubbed the "solvable splines" [58]. Their quadrupole formulation was described in Ref. [60]. They allow computing the thermal response of a multilayer made of graded layers, where the effusivity profile may be continuous up to the first or second derivative at each interface. Importantly, these analytical tools, in particular the PROFIDT approach, can be applied to wave equations as well. Their application to the Maxwell equations, in particular to modeling lightwave propagation in dielectrics with a graded refractive index, was described in Refs. [61], [62] and [63].
The "fundamental solutions" were briefly described in Ref. [58]. Although the related effusivity profiles do not present the same flexibility as that of the $\mathrm{sech}(\hat{\xi})$-type profiles, they are interesting for the reason that their shape (essentially concave or convex) can sometimes be quite acceptable for the considered task. In addition, the associated computation tools (namely the quadrupole matrix) are slightly simpler, as will be shown in this paper. The purpose of the present paper is to build upon the previous study and analyze in more detail the specific features of the "fundamental" effusivity profiles. In Section 2, we recall the method used to build solvable profiles in the Liouville space, together with their computational environment. Section 3 is devoted to linear profiles of $b^{1/2}(\xi)$ and $b^{-1/2}(\xi)$. Section 4 is devoted to hyperbolic and trigonometric profiles. In all cases, practical illustrations are provided in connection with a configuration of scientific and industrial interest, namely the system consisting of a substrate and a functionally graded coating such as those encountered in ceramic thermal barrier coatings. Section 5 is a discussion about other potential applications and a conclusion.

2. Solving the heat equation in the Liouville space

2.1. Two differential equations and their transformations

Consider a medium with temperature gradients in a single direction, say z (one-dimensional heat diffusion). In this direction, the thermal properties of the medium show continuous variations. The profile of thermal conductivity is $\lambda(z)$ and the profile of volumetric heat capacity (VHC) is $c(z)$. Therefrom are defined the profile of diffusivity: $a(z)=\lambda(z)/c(z)$ and the profile of effusivity: $b(z)=\sqrt{\lambda(z)c(z)}$. An exemplary situation is described in Fig. 1, where a layer of such material is used as a coating laid over a homogeneous substrate. In the Laplace or Fourier space, the heat equation for temperature (namely the heat equation in its classical form) is expressed as:

$$\langle T\rangle: \qquad pc(z)\theta=\frac{d}{dz}\left(\lambda(z)\frac{d\theta}{dz}\right) \tag{3}$$

Therein, for ease, p represents either the Laplace variable (for the purpose of analyzing the transient regime) or the Fourier variable $i\omega$ (for the purpose of analyzing the periodic regime), where ω is the angular frequency $2\pi f$ of the considered modulation (in that case, the $\exp(i\omega t)$ time-harmonic evolution is implicitly assumed throughout this paper). $\theta(z,p)$ is the Laplace or Fourier transform of the temperature $T(z,t)$; in Eq. (3) and in all other equations the independent variables will be generally omitted. This equation is denoted with the symbol $\langle T\rangle$, as will be done for any result derived therefrom.

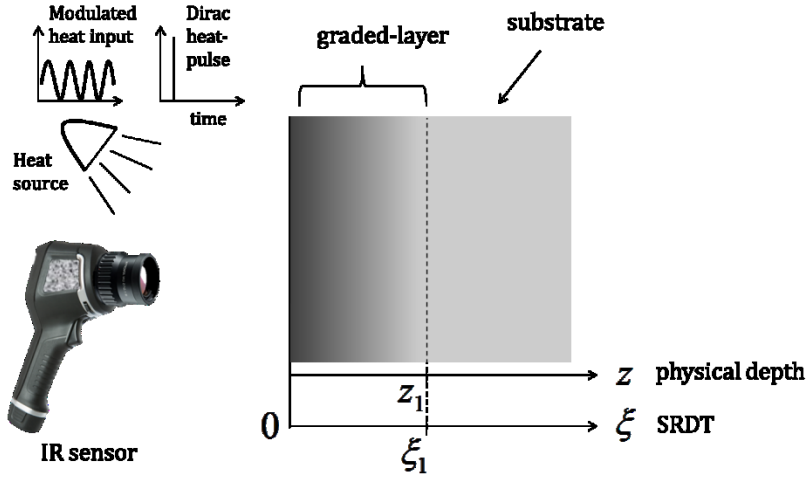

Fig. 1. Model of a continuously heterogeneous coating laid over a homogeneous substrate. The graded layer extends from $z=0$ to the depth $z=z_1$. In the SRDT space (Square Root of Diffusion Time) it extends from $\xi=0$ to $\xi=\xi_1$. A typical photothermal application is represented on the left, where a modulated or pulsed heat input is provided to the front surface of the coating, while an infrared sensor has been measuring the temperature variations of the front surface. This paper will present the results for different effusivity profiles in the coating.

A similar equation can be obtained for the heat-flux density and we will use, accordingly, the symbol $\langle\varphi\rangle$ ($\phi(z,p)$ is the Laplace or Fourier transform of the heat-flux density $\varphi(z,t)$):

$$\langle\varphi\rangle: \qquad p\frac{1}{\lambda(z)}\phi=\frac{d}{dz}\left(\frac{1}{c(z)}\frac{d\phi}{dz}\right) \tag{4}$$

Next, a Liouville transformation is applied, which first implies a change of the independent (space) variable $z\to\xi$, where ξ is defined by:

$$\xi\equiv\int_{z_0}^{z}a^{-1/2}(u)du \tag{5}$$

ξ corresponds to the square root of the diffusion time (SRDT) along the segment $[z_0, z]$, where z_0 is chosen arbitrarily (for ease, the origin of the z-scale is set at the left edge of the graded layer and z_0 is set to 0; in this way, the origin of the ξ-scale is also set at the left edge of the graded layer, - see Fig. 1).
The two heat equations in Eq. (3) and Eq. (4) become, in the new SRDT ξ-scale:

$$\langle T \rangle : \quad pb\theta = (b\theta')' \tag{6}$$

$$\langle \varphi \rangle : \quad pb^{-1}\phi = (b^{-1}\phi')' \tag{7}$$

where, and from now on, a prime denotes a derivation with respect to ξ.
The Liouville transformation also implies a change of the dependent variable θ, or respectively ϕ, by multiplying it by the function $s(\xi)$, which is alternatively defined by:

$$s(\xi) = b^{\pm 1/2}(\xi) \quad ; \quad \begin{cases} +1/2 & \text{in the } \langle T \rangle \text{ case} \\ -1/2 & \text{in the } \langle \varphi \rangle \text{ case} \end{cases} \tag{8}$$

A positive exponent refers to the $\langle T \rangle$-form equation, whereas a negative exponent refers to the $\langle \varphi \rangle$-form equation (this convention will apply throughout this paper, whenever a double-sign exponent is present). Due to this double representation with respect to effusivity, , $s(\xi)$ will be called a metaproperty.
Depending on the form of heat equation, the variable change is as follows:

$$\langle T \rangle : \quad \theta(\xi, p) \to \psi(\xi, p) : \quad \psi(\xi, p) = \theta(\xi, p) b^{+1/2}(\xi) \tag{9}$$

$$\langle \varphi \rangle : \quad \phi(\xi, p) \to \psi(\xi, p) : \quad \psi(\xi, p) = \phi(\xi, p) b^{-1/2}(\xi) \tag{10}$$

In each case, this leads to the *same differential equation*, which is a second-order equation in the so-called *Liouville normal form*:

$$\psi'' = (V(\xi) + p)\psi \quad ; \quad V(\xi) = \frac{s''(\xi)}{s(\xi)} \tag{11}$$

This also amounts to be a stationary Schrödinger equation with potential $V(\xi)$. Notice that the "Schrödinger" name is given to Eq. (11) just because of a formal similarity. However, no square-integrability condition applies to the (pseudo) wave-function ψ as in quantum mechanics. In addition, in the present context, solutions are sought for arbitrary values of the complex parameter p; there is no quest for eigenvalues or bound states as in quantum mechanics.

2.2. Preeminence of effusivity variations in the description of the thermal field

A first observation, as already mentioned in [58], is that the Liouville transformation offers the advantage of reducing the number of influential thermal profiles from two to one, namely from conductivity and VHC, in Eq. (3)-(4), to solely effusivity in Eq. (6)-(7). Furthermore, notice that the Fourier law is expressed in the ξ-space as: $\varphi = -bT'$, which means that conductivity has been "replaced" by effusivity (the same applies, of course, in the Laplace-Fourier space: $\phi = -b\theta'$). This is simply a consequence of the fact that the temperature gradient is now expressed in the ξ-scale, not in the z-scale. Hence, any boundary condition involving the conduction heat flux will be expressed in the ξ-space with effusivity and no other thermal property. Finally, stretching the (depth) z-scale into the (SRDT) ξ-scale has allowed the conductivity and heat capacity profiles to be merged into a unique influential profile, namely the effusivity $b(\xi)$. This underlines the unique role played by effusivity in the dynamic development of the temperature field. A direct consequence is that when comparing the response of two materials to a same heat load (i.e., same boundary condition type and same ξ-distribution of heat sources), the corresponding temperature distributions are different if and only if the effusivity profiles are themselves different. If the diffusivity z-profiles are different while the effusivity profiles $b(\xi)$ remain the same, this simply implies a spatial stretching of one temperature field relative to the other (note that diffusivity is actually embedded in the ξ variable).

Remember that this analysis is valid for *one-dimensional* heat transfer only; otherwise, the influence of the heterogeneous properties is more intricate.

2.3. General solution and quadrupole method

Basically, the problem comes down to finding mathematical functions $s(\xi)$ ensuring the integrability of the Schrödinger equation in Eq. (11). These will be called *solvable* $s(\xi)$-profiles. Those leading to solutions expressible in closed form and involving only elementary functions will, of course, be preferred.
The general solution to Eq. (11) will then be expressed as a linear combination (LC) of two linearly independent solutions (LIS), $K(\xi,p)$ and $P(\xi,p)$, which will be written as:

$$\psi(\xi,p) \propto \begin{bmatrix} K(\xi,p) \\ P(\xi,p) \end{bmatrix} \tag{12}$$

Generally speaking, the two multiplicative constants affecting $K(\xi,p)$ and $P(\xi,p)$ can be obtained by expressing the thermal boundary conditions prevailing at the boundaries of the considered graded layer in terms of the field function $\psi(\xi,p)$ and its derivative. Nevertheless, and especially in the presence of a multilayer, a very convenient way to calculate the temperature or the heat flux at one of the external or internal boundaries is to apply the quadrupole method [55], [56].
Quadrupoles $\mathbf{M}_{\langle T\rangle}$ and $\mathbf{M}_{\langle \varphi\rangle}$ are related, respectively, to profiles of $\langle T\rangle$-form or of $\langle \varphi\rangle$-form. How to build them, knowing two LIS solutions $K(\xi,p)$ and $P(\xi,p)$ associated with the effusivity profile under study, has been outlined in Ref. [58]. This methodology has been recalled in Appendix A. Practical applications will be described later in relation to the class of solvable effusivity profiles that are the subject of this paper.

2.4. Liouville inverse transformation

When it is necessary to go from the ξ-space back into the z-space, which constitutes the *inverse Liouville transformation*, a kind of indeterminacy appears. This indeterminacy should, however, be considered as a benefit. In essence, any solvable effusivity profile in the Liouville space, $b(\xi)$, can be associated with an infinite number of effusivity profiles in the depth space, $b(z)$, as becomes evident when inverting Eq. (5). This equation involves the diffusivity distribution, which implies that the result will depend on what is considered for it or, equivalently, as will be seen in the following, on what is considered for the distribution of any of the two remaining parameters: conductivity or VHC. Accordingly, the related temperature solution $\theta(\xi,p)$ can be associated with a plurality of solutions in the z-space: $\theta(z,p)$. The same thing happens for the heat flux (how to obtain $\theta(\xi,p)$ and $\phi(\xi,p)$ from $\psi(\xi,p)$ is fully described in Eq. (A-1)).
Nevertheless, one should be aware that it is only a matter of *distributing differently* the effusivity and temperature values, respectively $b(\xi)$ and $\theta(\xi,p)$, by *local stretching or compression* along the spatial scale. In any case, supplementary information is needed to perform the scale change $\xi \to z$. The relationship between the two scales is basically the one expressed in Eq. (5). If preferred, two additional equivalent expressions can be considered by replacing $a^{-1/2}(z)$ by $c(z)/b(z)$ or $b(z)/\lambda(z)$. Hence, from any profile $a(z)$, $c(z)$ or $\lambda(z)$, a profile $b(z)$ can be obtained that corresponds to the profile $b(\xi)$ initially obtained in the Liouville space; it is simply a case of selecting among the three expressions below the one that corresponds to the information input:

$$b(z) = b(\xi(z)) \quad ; \quad \begin{cases} \xi(z) = \int_0^z a^{-1/2}(u)\,du \\ \text{or} \quad \xi(z) = \int_0^z c(u) b^{-1}(u)\,du \\ \text{or} \quad \xi(z) = \int_0^z b(u) \lambda^{-1}(u)\,du \end{cases} \tag{13}$$

Note that, for the second and third choices, the effusivity profile $b(z)$ that we are seeking also appears in the integrand. The definition of $b(z)$ is then recursive, which would require iterations for its evaluation.
Another approach consists in capitalizing on the inverse of Eq. (5), which is given below through three equivalent expressions:

$$z = z(\xi) = \int_0^{\xi} a^{1/2}(u)du = \int_0^{\xi} b(u)c^{-1}(u)du = \int_0^{\xi} \lambda(u)b^{-1}(u)du \tag{14}$$

Hence, given a profile $a(\xi)$, $c(\xi)$ or $\lambda(\xi)$, one can obtain, after computing the corresponding quadrature, an explicit relationship between the two scales, namely through the function $z(\xi)$. Thereafter, the joint expressions of $z(\xi)$ and $b(\xi)$ provide a parametric definition (i.e., through ξ) of the effusivity profile in the z–scale. However, one could fear that the formal procedure described in Eq. (14) may be of limited use, since in most situations the profiles $a(\xi)$, $c(\xi)$ or $\lambda(\xi)$ are out of reach. Hopefully, important exceptions exist, namely when one or the other of these three parameters is known to be constant (actually, the case of constant diffusivity is trivial, since then the z–scale and the ξ–scale are simply proportional). Moreover, Eq. (14) can be replaced by a more general expression:

$$z = z(\xi) = \int_0^{\xi} a^{1/2}(u)du = \int_0^{\xi} \lambda^q(u)c^{q-1}(u)b^{1-2q}(u)du \quad ; \quad q \in \Re \tag{15}$$

Then, if $\lambda^q(z)c^{q-1}(z)$ happens to be constant for a particular value of the constant parameter q (the cases $q=0$, $q=1/2$ and $q=1$ correspond, respectively, to constant VHC, constant diffusivity and constant conductivity), the integral in Eq. (15) amounts to calculating the primitive of $b^{1-2q}(\xi)$:

$$z = \lambda_0^q c_0^{q-1} \int_0^{\xi} b^{1-2q}(z)du \quad ; \quad \lambda^q(z)c^{q-1}(z) = cst = \lambda_0^q c_0^{q-1} \tag{16}$$

For some of the solvable profiles that will be presented later, this quadrature can be expressed analytically, at least for some particular values of the parameter q.

2.5. Present scope: solutions stemming from a constant potential $V(\xi)$

Simple solutions to Eq. (11) can be obtained by choosing a constant potential: $V(\xi) = \beta = cst$. Depending on whether this constant is 0, strictly negative or strictly positive, this leads to a function $s(\xi)$ of either linear, trigonometric or hyperbolic type. The corresponding solvable effusivity profiles are obtained, according to Eq. (8), as the square of the aforementioned functions, or of their reciprocal. These profiles and the corresponding field solutions were briefly outlined in Ref. [58]. They generalize, for *arbitrary diffusivity* profiles, the solutions presented in Ref. [20]for *constant diffusivity* only. Furthermore, the solutions are *doubled* as a result of exploring the $\langle\varphi\rangle$-form equation in addition to the classical $\langle T\rangle$-form equation. Their counterparts for the wave equation have also been briefly outlined in Ref. [61]; they generalize those presented in Refs. [64] and [65] by considering arbitrary incidence and polarization, not only normal incidence.
The solutions stemming from a constant potential have been presented in [58] and [61] as "fundamental solutions", which were then used as seed solutions for the PROFIDT method (PROperty and FIeld Darboux Transformation). Our objective here is to go deeper into the analysis of these fundamental solutions, which, despite a remarkable simplicity, show a great interest for modeling graded layers, in particular coatings. We will provide the necessary tools for an easy implementation, in particular the quadrupole formulations, both for $\langle T\rangle$-form and $\langle\varphi\rangle$-form profiles.

3. Fundamental solutions obtained from a constant potential

We will distinguish the three cases: $V(\xi)=0$, $V(\xi)=\beta>0$ and $V(\xi)=\beta<0$. Most of the discussion will deal with graded layers of finite thickness. At the two positions $\xi=0$ and $\xi=\xi_1$ of the graded layer, the effusivity is assumed to reach, respectively, the values b_0 and b_1 (see Fig. 1).

3.1. Nil potential, $V(\xi)=0$; linear profiles for the metaproperty $s(\xi)$

3.1.1. Effusivity profiles in the Liouville-space

The solutions for $s(\xi)$ are the linear functions of the SRDT ξ. The corresponding effusivity profiles are defined by:

$$s(\xi)\equiv b^{\pm 1/2}(\xi)\propto\begin{bmatrix}B(\xi)\\D(\xi)\end{bmatrix}\equiv\begin{bmatrix}1\\\xi\end{bmatrix} \tag{17}$$

Let us recall that the plus sign in the exponent refers to the $\langle T\rangle$-form solution and the minus sign refers to the $\langle\varphi\rangle$-form solution. Due to the positivity constraint on the result of the linear combination in Eq. (17) (since $s(\xi)$ represents either the square root of effusivity or its reciprocal), if these profiles are to be used on the semi-infinite interval $\xi\in[0,+\infty]$, they should be restricted to $b(\xi)=(A_B+A_D\xi)^{\pm 2}$ with $A_B\geq 0$ and $A_D\geq 0$. $\langle T\rangle$-form profiles are then unbounded at $\xi\to+\infty$, whereas $\langle\varphi\rangle$-form profiles present a vanishing effusivity.

Let us now focus on finite-thickness layers. Taking into account the boundary values of effusivity, b_0 on the left, and b_1 on the right, the profiles are expressed as follows (by selecting the positive exponents for the $\langle T\rangle$-form profiles, and the negative exponents for the $\langle\varphi\rangle$-form profiles):

$$b(\xi)=\left[b_0^{\pm 1/2}\left(1-\frac{\xi}{\xi_1}\right)+b_1^{\pm 1/2}\frac{\xi}{\xi_1}\right]^{\pm 2} \tag{18}$$

A few profiles of $s(\xi)$, normalized by the left value s_0, have been plotted in Fig. 2. The ratio $(s_1/s_0)^2$ has been given four values between 1.25 and 4 and their reciprocal. The particular case where the metaproperty vanishes on the right, i.e., $s_1=0$, has also been added (lower curve). The corresponding profiles of $b(\xi)$ have been plotted in Fig. 3 for both the $\langle T\rangle$-form and $\langle\varphi\rangle$-form cases, which means that, respectively, $b(\xi)=s^2(\xi)$ and $b(\xi)=s^{-2}(\xi)$. Normalization by the left-edge value b_0 has been introduced. For any value of b_1/b_0 except 0, we thus obtain a set of two solvable profiles, one of $\langle T\rangle$-form and one of $\langle\varphi\rangle$-form (see each pair of black and red curves in Fig. 3). These partner profiles differ more and more from each other as the ratio b_1/b_0 becomes progressively larger or smaller than 1.

In the limiting case where effusivity vanishes at one boundary, namely b_1=0, only the $\langle T\rangle$-form solution is retained and the profile expression is: $b(\xi)=b_0(1-\xi/\xi_1)^2$ (bottom black dashed curve). The $\langle\varphi\rangle$-form profiles in Fig. 3 (red curves) have a limiting curve for $b_1/b_0\to\infty$, which has been drawn in red dashed line. The (normalized) profile expression is simply the reciprocal of the previous one, namely $b(\xi)=b_0(1-\xi/\xi_1)^{-2}$. These two solutions are mathematical asymptotical limits intended to model situations where the product of conductivity and VHC decreases to very low values (as could be observed with a strong-porosity gradient), or conversely increases to very high values (as for example in a composite material with an increasing density of metallic particles, up to percolation).

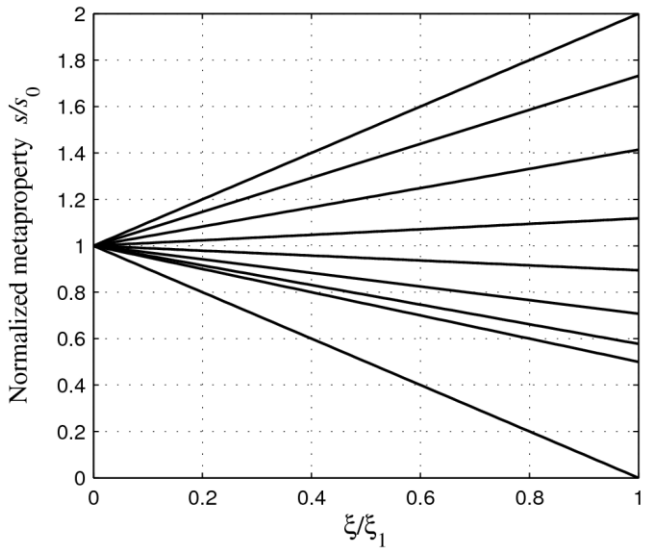

Fig. 2. Linear profiles of the metaproperty $s(\xi)=b(\xi)^{\pm 1/2}$. The $s(\xi)$ function is normalized by the value s_0 taken at the left boundary, i.e., at $\xi=0$. It has been plotted as a function of the Liouville variable ξ (square root of the diffusion time - SRDT), which has been normalized by the value corresponding to the layer thickness, ξ_1. From bottom to top, the right-to-left ratio $(s_1/s_0)^2$ takes the values 0, 0.25, 1/3, 0.5, 0.8, 1.25, 2, 3, 4.

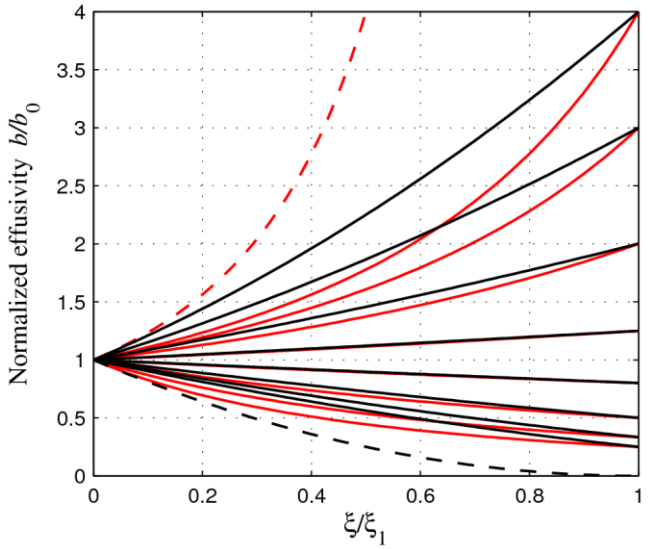

Fig. 3. Fundamental effusivity profiles $b(\xi)$ corresponding to the linear profiles in Fig 2 of the metaproperty $s(\xi)=b(\xi)^{\pm 1/2}$. Effusivity is normalized by the value b_0 taken at the left boundary. It has been plotted in function of the normalized SRDT, i.e., ξ/ξ_1. From bottom to top, the right-to-left effusivity ratio b_1/b_0 takes the values 0, 0.25, 1/3, 0.5, 0.8, 1.25, 2, 3, 4. Except for b_1=0, there are two solutions: one of $\langle T\rangle$-form (in black) and one of $\langle\varphi\rangle$-form (in red). For b_1=0, there is only one solution of $\langle T\rangle$-form (in dashed-black). The top dashed-red curve is a $\langle\varphi\rangle$-form profile corresponding to the asymptotic case $b_1/b_0\to\infty$.

3.1.2. Thermal-property profiles in the z-space

Each curve in Fig. 3 is subject to an arbitrary multiplicity in the physical-depth space (see the discussion on the Liouville inverse transformation in § 2.4). In particular, if we assume that $\lambda^q(z)c^{q-1}(z)$ is constant for some value of the exponent q, it can be shown that the effusivity profiles $b(z)$ and all other properties $\lambda(z)$, $c(z)$ and $a(z)$ are expressed in the physical-depth space in the same generic form:

$$\Gamma(z)=\left[\Gamma_0^{1/r}\left(1-\frac{z}{z_1}\right)+\Gamma_1^{1/r}\frac{z}{z_1}\right]^r \tag{19}$$

where Γ stands for b,λ,c or a, and the expression of the exponent r differs depending on the considered thermal parameter (which appears thereafter as a subscript of r):

$$\begin{matrix} r_b=\pm 2/m & ; & r_\lambda=\pm 4(1-q)/m \\ r_c=\pm 4q/m & ; & r_a=\pm 4(1-2q)/m \end{matrix} \quad ; \quad m=1\pm 2(1-2q) \tag{20}$$

In addition, the right-to-left ratio of each of the three remaining properties is obtained from b_1/b_0, according to:

$$\lambda_1/\lambda_0=(b_1/b_0)^{2(1-q)}; \quad c_1/c_0=(b_1/b_0)^{2q}; \quad a_1/a_0=(b_1/b_0)^{2(1-2q)} \tag{21}$$

Three important subcases are described thereafter. First a constant VHC ($q=0$):

$$\langle T\rangle: \quad \begin{cases} b(z)=\left[b_0^{3/2}(1-z/z_1)+b_1^{3/2}\,z/z_1\right]^{2/3} \\ \lambda(z)=\left[\lambda_0^{3/4}(1-z/z_1)+\lambda_1^{3/4}\,z/z_1\right]^{4/3} \\ a(z)=\left[a_0^{3/4}(1-z/z_1)+a_1^{3/4}\,z/z_1\right]^{4/3} \end{cases} \qquad \langle\varphi\rangle: \quad \begin{cases} b(z)=\left[b_0^{1/2}(1-z/z_1)+b_1^{1/2}\,z/z_1\right]^{2} \\ \lambda(z)=\left[\lambda_0^{1/4}(1-z/z_1)+\lambda_1^{1/4}\,z/z_1\right]^{4} \\ a(z)=\left[a_0^{1/4}(1-z/z_1)+a_1^{1/4}\,z/z_1\right]^{4} \end{cases} \tag{22}$$

then, a constant diffusivity ($q=1/2$):

$$\langle T\rangle: \quad \begin{cases} b(z)=\left[b_0^{1/2}(1-z/z_1)+b_1^{1/2}\,z/z_1\right]^{2} \\ \lambda(z)=\left[\lambda_0^{1/2}(1-z/z_1)+\lambda_1^{1/2}\,z/z_1\right]^{2} \\ c(z)=\left[c_0^{1/2}(1-z/z_1)+c_1^{1/2}\,z/z_1\right]^{2} \end{cases} \qquad \langle\varphi\rangle: \quad \begin{cases} b(z)=\left[b_0^{-1/2}(1-z/z_1)+b_1^{-1/2}\,z/z_1\right]^{-2} \\ \lambda(z)=\left[\lambda_0^{-1/2}(1-z/z_1)+\lambda_1^{-1/2}\,z/z_1\right]^{-2} \\ c(z)=\left[c_0^{-1/2}(1-z/z_1)+c_1^{-1/2}\,z/z_1\right]^{-2} \end{cases} \tag{23}$$

and finally a constant conductivity ($q=1$):

$$\langle T\rangle: \quad \begin{cases} b(z)=\left[b_0^{-1/2}(1-z/z_1)+b_1^{-1/2}\,z/z_1\right]^{-2} \\ a(z)=\left[a_0^{1/4}(1-z/z_1)+a_1^{1/4}\,z/z_1\right]^{4} \\ c(z)=\left[c_0^{-1/4}(1-z/z_1)+c_1^{-1/4}\,z/z_1\right]^{-4} \end{cases} \qquad \langle\varphi\rangle: \quad \begin{cases} b(z)=\left[b_0^{-3/2}(1-z/z_1)+b_1^{-3/2}\,z/z_1\right]^{-2/3} \\ a(z)=\left[a_0^{3/4}(1-z/z_1)+a_1^{3/4}\,z/z_1\right]^{4/3} \\ c(z)=\left[c_0^{-3/4}(1-z/z_1)+c_1^{-3/4}\,z/z_1\right]^{-4/3} \end{cases} \tag{24}$$

As an illustration, let us perform an inverse Liouville transformation on the two profiles $b(\xi)$ in Fig. 3 that correspond to the particular case b_1/b_0 =3 (the one of $\langle T\rangle$-form, in black, and the one of $\langle\varphi\rangle$-form, in red). Different values have been given to the exponent q between -1 and +2, in steps of 0.25. A double series of sets of four profiles $b(z)$, $\lambda(z)$, $c(z)$ and $a(z)$ are thus obtained in the physical-depth space, as reported in Figs. 4 to 7.

Notice that the illustration given in Figs. 4 to 7 is rather formal; as a matter of fact, the graded parameters $\lambda(z)$, $c(z)$ and $a(z)$ present fairly large variations for the most extreme values of the exponent q. In any case, let us recall that in Figs. 4 to 7, all four-profile sets in the z-space of a given form, $\langle T\rangle$ or $\langle\varphi\rangle$, (i.e., all profiles of the same color), are associated with a *single temperature field* $\theta(\xi,p)$ (for a given set of boundary conditions), since they originate from the same *effusivity profile* $b(\xi)$.

Interestingly enough, two effusivity profiles $b(z)$ of $\langle T\rangle$-form and of $\langle\varphi\rangle$-form obtained with exponents q_T and q_φ, such that $q_T-q_\varphi=1/2$ perfectly overlap in the z-space (see Fig. 4).

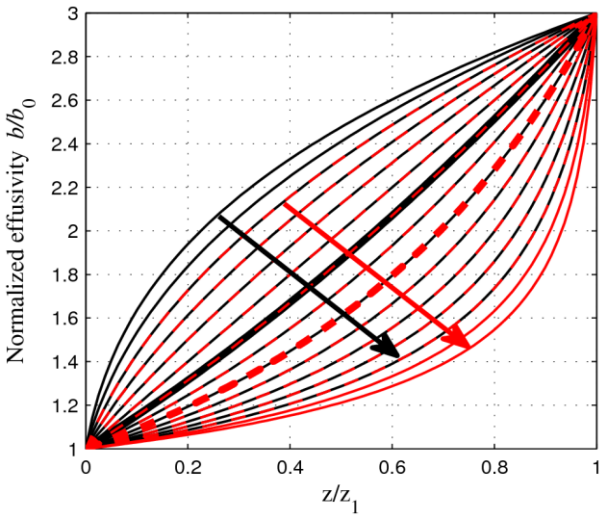

Fig. 4. Fundamental profiles of effusivity in the z-space, i.e., $b(z)$, as obtained after an inverse Liouville transformation. All profiles of $\langle T \rangle$-form (in black) originate from the profile $b(\xi)$ in Fig. 3 with b_1/b_0 =3 and $\langle T \rangle$-form. The same applies for the $\langle \varphi \rangle$-form profiles in red. The arrows indicate a growing value of the exponent q, from -1 to +2 in steps of 0.25 (see Eqs. (15)-(16) and Eqs. (19)-(21)). A profile of $\langle T \rangle$-form and a profile of $\langle \varphi \rangle$-form overlap when the former q_T value is 0.5 higher than the latter value q_φ (the red and black curves are then dashed). Profiles obtained with q =0.5 (constant diffusivity) are drawn with a bold line (they have the same shape as in the ξ-space; see Fig. 3).

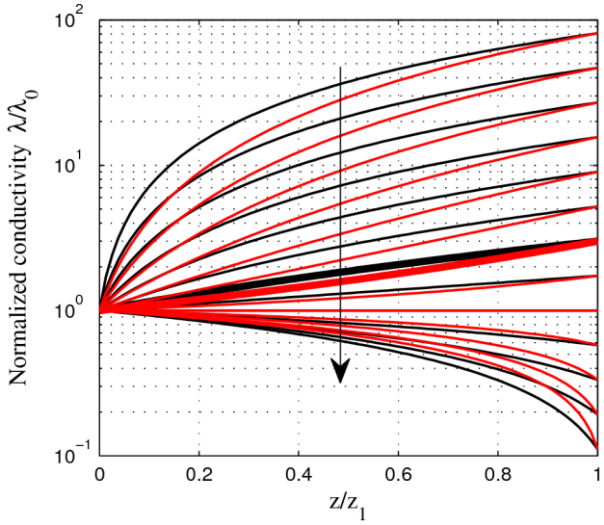

Fig. 5. Same as in Fig. 4 for the thermal conductivity. The arrow indicates a growing value of the exponent q, for the $\langle T \rangle$-form profiles (in black) and the $\langle \varphi \rangle$-form profiles (in red).

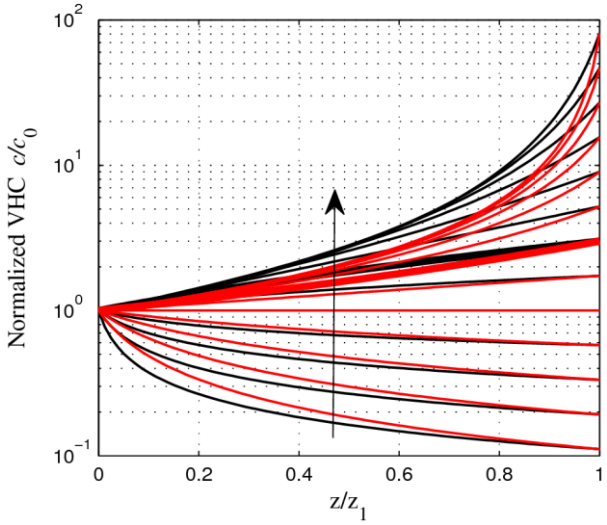

Fig. 6. Same as in Fig. 5 for the volumetric heat capacity (VHC).

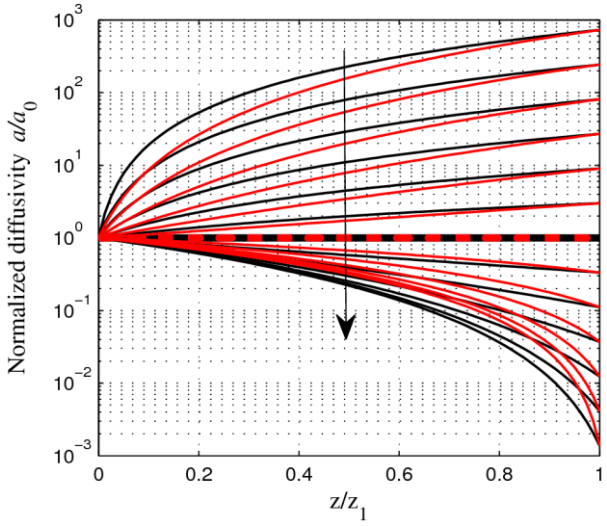

Fig. 7. Same as in Fig. 5 for the diffusivity.

3.1.3. Quadrupoles associated with the linear profiles

The generic field function is obtained as a LC of the hyperbolic sine and cosine functions of the argument $\sqrt{p}\xi$:

$$\psi(\xi,p)\propto\begin{bmatrix}K(\xi,p)\\P(\xi,p)\end{bmatrix}\equiv\begin{bmatrix}C^{(0)}(\xi)\\S^{(0)}(\xi)/\sqrt{p}\end{bmatrix}\quad;\quad\begin{bmatrix}C^{(0)}(\xi)\\S^{(0)}(\xi)\end{bmatrix}\equiv\begin{bmatrix}\cosh\left(\sqrt{p}\xi\right)\\\sinh\left(\sqrt{p}\xi\right)\end{bmatrix}\tag{25}$$

It is then easy to calculate the five terms in Eq. (A-5) that intervene in the quadrupole expression:

$$\begin{cases}G=\cosh\left(\sqrt{p}\xi_1\right) & ;\quad H=-\cosh\left(\sqrt{p}\xi_1\right)\\ I=\sinh\left(\sqrt{p}\xi_1\right)/\sqrt{p} & ;\quad J=-\sqrt{p}\sinh\left(\sqrt{p}\xi_1\right)\\ \Delta=1\end{cases}\tag{26}$$

where ξ_1 represents the square root of the total diffusion time through the graded layer, i.e., according to Eq. (5): $\xi_1=\int_0^{z_1}a^{-1/2}(u)du$. Following the procedure described in Eq. (A-4), we obtain the four entries of the quadrupole $\mathbf{M}_{\langle T\rangle}$, as presented thereafter in a non-dimensional form:

$$\begin{bmatrix} A \\ B \\ C \\ D \end{bmatrix} = \begin{bmatrix} 1 \\ \xi_1/(s_0 s_1) \\ s_0 s_1/\xi_1 \\ 1 \end{bmatrix} \bullet \left(\begin{bmatrix} x & 1-x \\ 0 & 1 \\ (x-1)(1-x^{-1}) & p\xi_1^{\,2} - (x-1)(1-x^{-1}) \\ x^{-1} & 1-x^{-1} \end{bmatrix} \times \begin{bmatrix} \cosh\left(\sqrt{p}\xi_1\right) \\ \dfrac{1}{\sqrt{p}\xi_1}\sinh\left(\sqrt{p}\xi_1\right) \end{bmatrix} \right) \quad ; \quad x \equiv \frac{s_1}{s_0} \tag{27}$$

knowing that for a $\langle T \rangle$-form profile, the substitution $s_{0,1} \leftarrow b_{0,1}^{\,+1/2}$ should be made. To obtain the quadrupole matrix $\mathbf{M}_{\langle \varphi \rangle}$ related to a $\langle \varphi \rangle$-form profile, the substitution $s_{0,1} \leftarrow b_{0,1}^{\,-1/2}$ should be made, and then the permutation rule described in Eq. (A-6) should be applied. In Eq. (27), the symbol × denotes a matrix product, whereas • denotes a term by term product (i.e., line by line).

When $x \equiv s_1/s_0 = 1$, both $\langle T \rangle$-form and $\langle \varphi \rangle$-form profiles merge into a constant profile ($b_1 = b_0$) and it is easy to check that the previous relationship becomes:

$$\begin{bmatrix} A \\ B \\ C \\ D \end{bmatrix} = \begin{bmatrix} 1 \\ \xi_1/b_0 \\ b_0/\xi_1 \\ 1 \end{bmatrix} \bullet \left(\begin{bmatrix} 1 & 0 \\ 0 & 1 \\ 0 & p\xi_1^{\,2} \\ 1 & 0 \end{bmatrix} \times \begin{bmatrix} \cosh\left(\sqrt{p}\xi_1\right) \\ \dfrac{1}{\sqrt{p}\xi_1}\sinh\left(\sqrt{p}\xi_1\right) \end{bmatrix} \right) \tag{28}$$

which effectively corresponds to the quadrupole expression of a layer with constant effusivity b_0 and SRDT ξ_1. If diffusivity is also a constant, i.e., $a(z) = \overline{a}$, then we have $\xi_1 = z_1 \overline{a}^{\,-1/2}$ and we retrieve the classical quadrupole expression of a homogeneous layer [55].

3.1.4. Temperature computations

The results that will be presented first are aimed at simulating the radiometric photothermal response of a graded coating of "linear" type when laid over a very thick and homogeneous substrate. The front face of the coating, where effusivity takes the value b_0, is subjected to a heat source of power density $\wp(p)$ (in the Laplace-Fourier space). The rear face of the coating, where the effusivity reaches the value b_1, is backed by a semi-infinite homogeneous layer having the same effusivity b_1. When the free surface of the coating is submitted to linear heat losses with coefficient h (boundary condition of the third type), the temperature response at this free surface is given by (see, for example, Refs. [55], [56] and [66], and references therein):

$$\theta_0 = \wp \frac{AZ + B}{CZ + D + h(AZ + B)} \tag{29}$$

where *A, B, C, D* are the quadrupole entries of the coating (Eq. (27)) and Z is the thermal impedance of the substrate; i.e., $Z = \left(b_1\sqrt{p}\right)^{-1}$. The following examples will, however, be restricted to the adiabatic case; i.e., h=0. The first results correspond to the periodic case (modulated heat source of power-density magnitude P - not to be confused with the independent solution in Eq. (12) - and angular frequency ω; the spectral variable p appearing in Eq. (29) should then be set to $i\omega$).

The results regarding the amplitude and phase of the surface temperature have been plotted in Fig. 8 and Fig. 9 for four values of the ratio b_1/b_0 : 1/3, 2/3, 3/2 and 3, and for both $\langle T \rangle$-form and $\langle \varphi \rangle$-form profiles. The frequency f has been normalized by ξ_1^{-2}, knowing that ξ_1^2 represents the diffusion time through each considered coating. The amplitude has been normalized by $P\xi_1/b_0$.

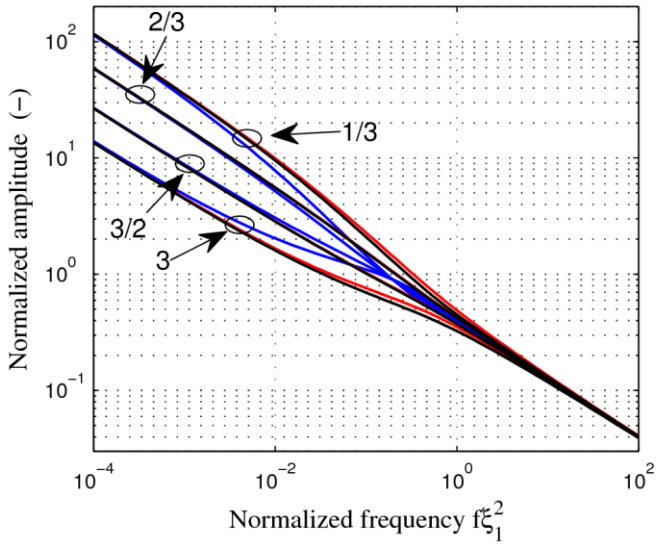

Fig. 8. Magnitude of the temperature periodic response at the free surface of a selection of eight "linear"-type *graded* coatings and four *homogeneous* coatings over a semi-infinite substrate with b_1/b_0 =1/3, 2/3, 3/2 and 3 (adiabatic bi-layers). The responses of the $\langle T \rangle$-form profiles are in black; those of the $\langle \varphi \rangle$-form profiles are in red (for a better discrimination, see Fig. 10 below). The curves in blue correspond to *homogeneous* coatings of effusivity b_0 laid over a substrate of effusivity b_1 [67]

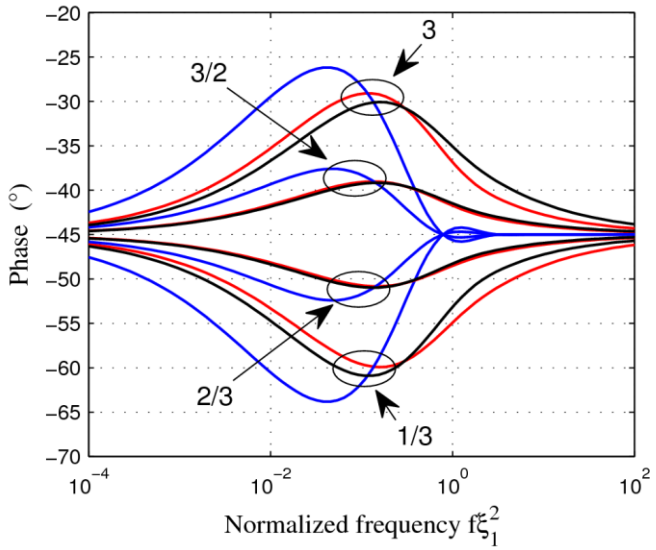

Fig. 9. Same as in Fig 8 for the phase of the temperature response.

For comparison, we also plotted (in blue) the classical response of a coating with constant effusivity b_0 [67]. To compute the response of the uniform coatings, the quadrupole entries *A, B, C, D* expressed in Eq. (28) simply have to be substituted into Eq. (29). In the latter case of a homogeneous coating, the effusivity presents a jump from b_0 to b_1 right at the interface. In the graded coating systems presented in this paper, the effusivity profile is continuous (albeit non-smooth) at the interface.

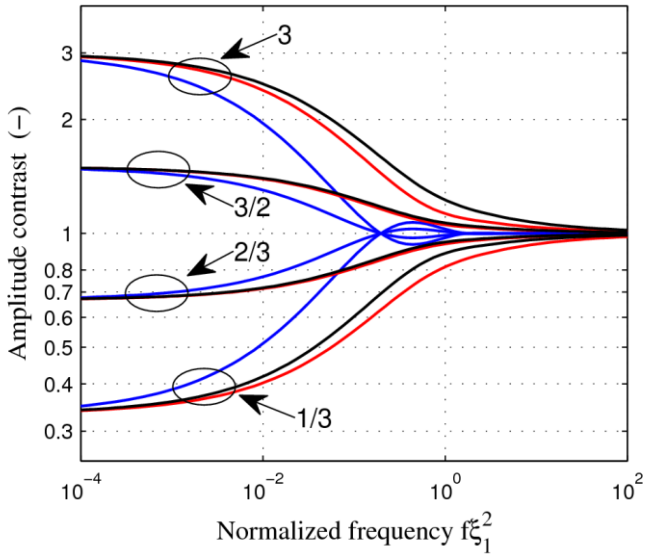

Fig. 10. Same as in Fig 8 for the inverse contrast of the amplitude with respect to a semi-infinite material with constant effusivity b_0. This observable can be interpreted as a (frequency-dependent) "apparent effusivity" normalized by b_0.

In Fig. 8, at low and high frequency, the temperature amplitude evolves asymptotically with the frequency as $f^{-1/2}$. On the other side, the temperature amplitude of a homogeneous semi-infinite layer of effusivity b_0 is $\left|\theta_0^{ref}\right| = P/\left(b_0\sqrt{2\pi f}\right)$. If we calculate the inverse contrast $\left|\theta_0^{ref}\right|/\left|\theta_0\right|$, we obtain another way of presenting the temperature amplitude, which is deprived of the $f^{-1/2}$ trend and which magnifies the differences between the coating responses (see Fig. 10). This is a frequency-dependent function whose asymptotic limits are 1 for $f \to \infty$ and b_1/b_0 for a vanishing frequency. It can be interpreted as a normalized *apparent effusivity*, i.e., $b_{app}(f)/b_0$ with $b_{app}(f) \xrightarrow[f\to\infty]{} b_0$ and $b_{app}(f) \xrightarrow[f\to 0]{} b_1$. This is the frequency-domain counterpart of the apparent effusivity initially defined in the time domain [68], and which will be discussed further on. This empirical observable has a potential for in-depth effusivity scanning. In other words, it provides a simple, yet quite crude, identification of the in-depth variations of effusivity. As a matter of fact, by sweeping from high-frequency to low-frequency values, progressively deeper values of the effusivity profile can be revealed. Of course, this approach is very approximate. This is confirmed through the homogeneous coating cases (blue curves). As a matter of fact, the effusivity jump at the interface between the coating and the substrate is not reflected in the curves of the apparent effusivity. The transition is much smoother. Moreover, even slight undulations are noticed when the normalized frequency is in the range 0.1-1. Similar undulations are also observed in the phase plot (Fig. 9) and they are classically interpreted as the result of "interferences" of the so-called "thermal wave". It should also be noted that the (normalized) apparent effusivity comes close to the value representative of the substrate, namely b_1/b_0, only for very low values of the normalized frequency (less than 10^{-2}, or even 10^{-3}, depending on the acceptance criterion).

When considering the coatings with a graded effusivity now, on the whole, the evolution with frequency of the amplitude response and the phase response is smoother, which is nothing unexpected (compare the black and red curves on the one hand and the corresponding blue curves on the other hand). On the other side, the previously mentioned undulations are now absent from the amplitude (and apparent-effusivity) curves as well as from the phase curves. Furthermore, when starting from high frequency values and moving downwards, the departure from the behavior of a material with constant effusivity b_0 is observed earlier with a graded coating, which, again, is quite natural, since effusivity starts changing immediately below the free surface.

The $\langle T \rangle$-form and $\langle \varphi \rangle$-form profiles present different responses. They compare differently, whether b_1/b_0 is larger or smaller than one. In the former case, i.e., for an increasing effusivity profile, the effusivity moves

faster from b_0 for a $\langle T \rangle$-form profile than it does for a $\langle \varphi \rangle$-form profile (see Fig. 3). In the latter case, i.e., for a decreasing effusivity profile, it is the contrary. This explains why, for b_1/b_0 >1 and when the frequency is decreasing, the resulting curves (phase or apparent effusivity) of a $\langle T \rangle$-form coating change faster than with a $\langle \varphi \rangle$-form profile. When b_1/b_0 <1, the opposite is observed.

Remarkable symmetry has been observed in the amplitude and phase responses for *homogenous* coatings when comparing systems with ratios b_1/b_0 that are the inverse of each other [67]. This means that the blue curves in the phase plot in Fig. 9 are symmetric with respect to the reference line at 45°. Similarly, the blue curves in the amplitude plot in Fig. 8 are (vertically) symmetric with respect to the reference line $1/\sqrt{\omega\xi_1^2}$, which makes the apparent-effusivity curves in Fig. 10 symmetric with respect to the reference line $b_{app}(f)/b_0 = 1$; i.e., they are the reciprocal of each other. The same symmetry can be observed for the graded coatings, provided that the $\langle T \rangle$-form and $\langle \varphi \rangle$-form profiles are exchanged when moving from a b_1/b_0 value to its reciprocal.

To obtain the transient response of a bi-layer system when it is submitted to a Dirac pulse of energy density Q, one simply needs to perform an inverse Laplace transform of Eq. (29) with $\wp(p) = Q$. In all likelihood, an analytical expression is beyond reach; we must therefore resort to a numerical approach, as for example the De Hoog method [72].

The adiabatic response of a homogeneous semi-infinite slab is $Q/b_0\sqrt{\pi t}$. When dividing it by the transient response of one of the considered bi-layers we obtain a *time-dependent* temperature contrast, which corresponds to (another) normalized *apparent effusivity*, i.e., $b_{app}(t)/b_0$ with $b_{app}(t) \xrightarrow[t\to 0]{} b_0$ and $b_{app}(t) \xrightarrow[t\to \infty]{} b_1$ [6], [66], [68], [69], [70], [71]. This temperature (relative) contrast has been plotted in Fig. 11 for the eight graded and four step-profile coating systems considered in Figs. 8-10. Let us now compare the "frequency-version" of the apparent effusivity in Fig. 10 and the "time-version" in Fig. 11.

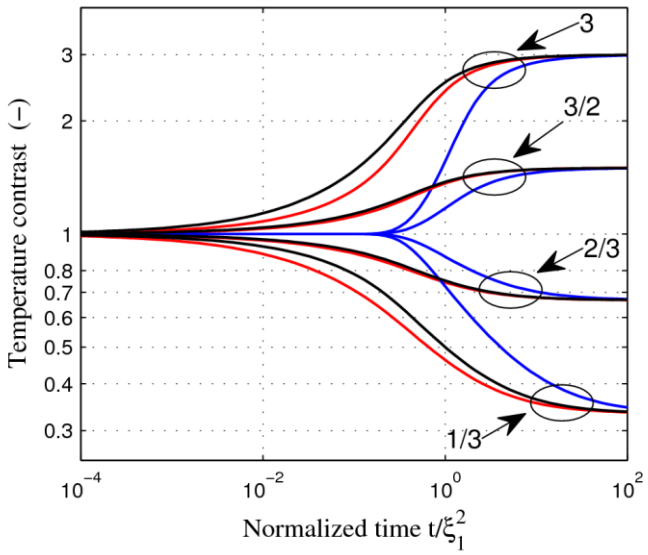

Fig. 11. Same as in Fig 10, in the time domain, when comparing the responses of the coating/substrate systems to a Dirac pulse. The temperature contrast is obtained by dividing the transient temperature of the surface of a material having a constant effusivity b_0 by the transient temperature of each considered bilayer. This observable can be interpreted as a (time-dependent) "apparent effusivity" normalized by b_0.

Broadly speaking, the comments on the results obtained in the frequency domain can be directly transposed in the time domain after reversing the frequency scale. There are, nevertheless, some important differences. The first point to notice is that the undulations in the blue curves related to the homogeneous coatings in Fig. 10 are absent in Fig. 11. Thus, in the time domain, it appears that a monotonically increasing/decreasing

effusivity profile gives rise to a similarly monotonically increasing/decreasing evolution of the apparent effusivity, which is obviously a good point. The second difference lies in the fact that the apparent-effusivity transition between b_0 and b_1 is far steeper in the time log-scale than in the frequency log-scale. This is particularly noticeable for the homogeneous-coating systems (blue curves). All of this means that the time response seems to provide a "clearer" and more faithful tomographic image of the subsurface effusivity profile than the frequency response does. Of course, this statement refers to the raw signals, which does not preclude that, after implementing *ad hoc* inversion strategies, the results are necessarily improved in both cases. Nevertheless, between modulated and pulsed experimental methodologies, it would be quite tempting to choose the latter, since it produces, from the outset, a signal of higher intrinsic quality regarding the potential for depth profiling.

Let us now consider the two limiting cases drawn with dashed lines in Fig. 3, namely $b_1 \to 0$ ($\langle T \rangle$-form) and $b_1 \to \infty$ ($\langle \varphi \rangle$-form). These graded layers should be considered on their own. The first one has a permanently null flux on its rear face, i.e. at $z = z_1$ (it will be assumed that the temperature derivative is bounded at this location), whereas the second one has a permanently null temperature. For that reason, the classical configuration with a homogeneous layer that will be compared with the limiting case $b_1 \to 0$ is obtained by imposing an adiabatic condition ($\varphi_1 = 0$) at the rear side of the homogeneous layer (condition of the second kind). Reciprocally, for the limiting case $b_1 \to \infty$, a condition of the first kind with $T_1 = 0$ will be applied.

The expression for the temperature in Eq. (29) is simplified as follows for the two graded layers:

$$\theta_0 = \frac{\wp}{b_0\sqrt{p}}\left[\frac{\sqrt{p}\xi_1}{\sqrt{p}\xi_1 \coth\left(\sqrt{p}\xi_1\right) - 1 + h\xi_1 b_0^{-1}}\right] \quad ; \quad b_1 \to 0 \tag{30}$$

$$\theta_0 = \frac{\wp}{b_0\sqrt{p}}\left[\frac{\sqrt{p}\xi_1}{\sqrt{p}\xi_1 \coth\left(\sqrt{p}\xi_1\right) - 1} + \frac{h}{b_0\sqrt{p}}\right]^{-1} \quad ; \quad b_1 \to \infty \tag{31}$$

In both cases, we can recognize the temperature of a homogeneous semi-infinite material of effusivity b_0 multiplied by a corrective term in brackets. One can notice that, in the adiabatic case (h=0), the corrective terms in Eq. (30) and Eq. (31) are the inverse of each other.

The front face temperature of a homogeneous layer with $\varphi_1 = 0$ at the rear side is simply $\theta_0 = \wp \coth\left(\sqrt{p}\xi_1\right) / \left(b_0\sqrt{p}\right)$. When $T_1 = 0$ at the rear side, it becomes $\theta_0 = \wp \tanh\left(\sqrt{p}\xi_1\right) / \left(b_0\sqrt{p}\right)$.

In Fig. 12 to 13, the amplitude and phase of the periodic response of the former graded and homogeneous slabs have been plotted.

The (frequency–dependent) apparent effusivity, as defined from the inverse amplitude contrast, is plotted in Fig. 14. The same as is obtained in the time domain when replacing the modulated heat source by a pulse source can be seen in Fig. 15.

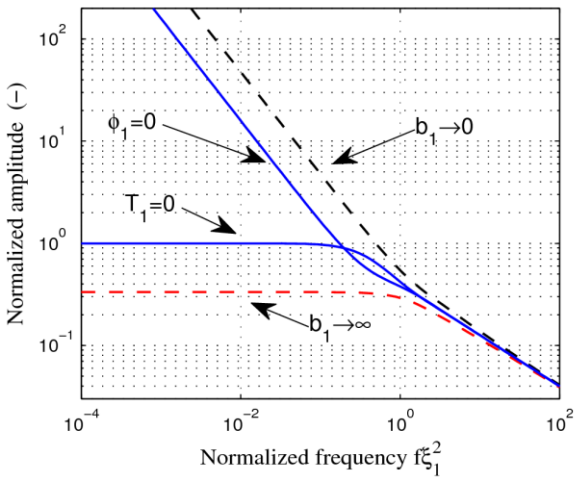

Fig. 12. Magnitude of the temperature periodic response at the front surface of a series of single layers. Dashed black line: "linear" graded layer with $b_1 \to 0$ ($\langle T \rangle$-form profile in Fig. 3 of same type and color). Dashed red line: "linear" graded layer with $b_1 \to \infty$ ($\langle \varphi \rangle$-form profilein Fig. 3 of same type and color). Blue lines: homogenous layers of effusivity b_0 with either $T_1 = 0$ (BC of the 1st kind) or $\varphi_1 = 0$ (BC of the 2nd kind) at the back face.

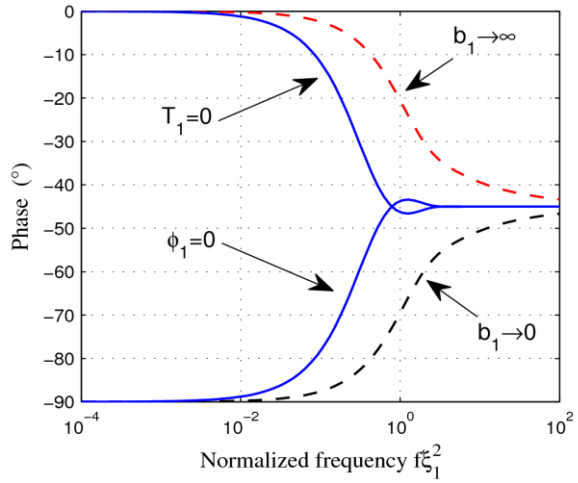

Fig. 13. Same as in Fig. 12 for the phase.

The results for the homogeneous slabs are well known and do not need any comment. Regarding the "linear"-type layers, a general remark is that, on the whole, the departure from the homogeneous, semi-infinite case and the entry into the "deep" asymptotic behavior is observed sooner, which means at a higher value of the decreasing frequency, or a smaller value of the increasing time. In addition, all observables (amplitude, phase and both apparent effusivities) are monotonically increasing or decreasing. The asymptotic limits for the phase are the same as those for the corresponding homogeneous slabs.

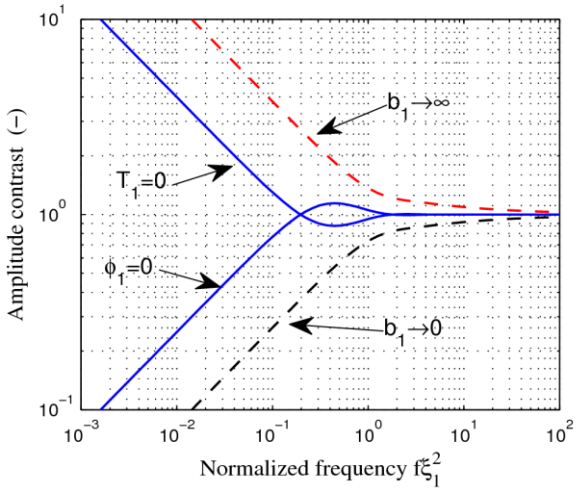

Fig. 14. Same as in Fig. 12 for the amplitude inverse contrast with respect to a semi-infinite material with constant effusivity b_0.

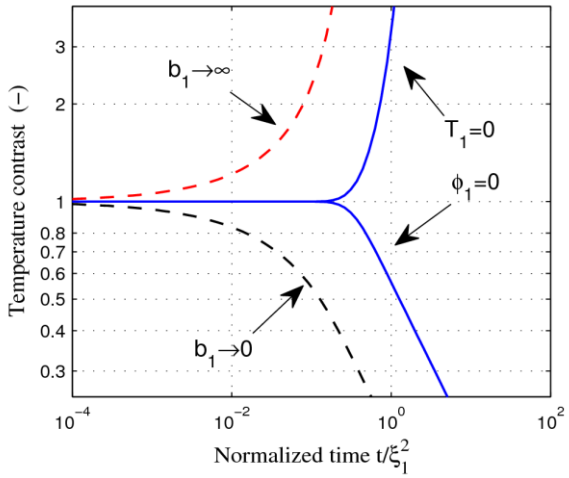

Fig. 15. Same as in Fig 14 in the time domain when comparing the responses obtained with a Dirac pulse.

3.2. Positive or negative potential, $V(\xi)=\beta\neq 0$; hyperbolic and trigonometric profiles for $s(\xi)$

3.2.1. Effusivity profiles in the Liouville-space

Let us introduce ξ_c, which is defined by $\xi_c \equiv 1/\sqrt{|\beta|}$, where β represents the positive or negative value chosen for the constant potential $V(\xi)$; $\xi_c^{\,2}$ represents a characteristic diffusion-time of the graded profile. When $\beta>0$, the solutions for the metaproperty $s(\xi)$ are LCs of the exponential functions of $+\xi/\xi_c$ and $-\xi/\xi_c$ or, equivalently, LCs of the hyperbolic cosine and hyperbolic sine functions of ξ/ξ_c. When $\beta>0$, the solutions are LCs of the cosine and sine functions of ξ/ξ_c. The corresponding effusivity profiles are thus obtained from:

$$b^{\pm 1/2}(\xi)=A_B B(\xi)+A_D D(\xi) \quad ; \quad \begin{bmatrix} B(\xi) \\ D(\xi) \end{bmatrix} \equiv \begin{cases} \begin{bmatrix} \cosh(\xi/\xi_c) \\ \sinh(\xi/\xi_c) \end{bmatrix} & \text{if } \beta>0 \\ \begin{bmatrix} \cos(\xi/\xi_c) \\ \sin(\xi/\xi_c) \end{bmatrix} & \text{if } \beta<0 \end{cases} \tag{32}$$

These profiles encompass those presented in Ref. [20], which were restricted to constant diffusivity. They also encompass the exponential profiles $b(\xi) = b_0 \exp(\pm \xi/\xi_c)$ presented in Refs. [52] and [53].

Due to the positivity constraint on the result of any linear combination in Eq. (32), the second option ($\beta < 0$) can be applied only over a finite interval, $\xi \in [0, \xi_1]$, whereas the first option could be applied over a finite or semi-infinite interval. In the latter case, the only $\langle T \rangle$-form profiles that are bounded are of the type $b(\xi) = b_0 \exp(-2\xi/\xi_c)$, whereas those of $\langle \varphi \rangle$-form are of the type

$b(\xi) = [A_B \exp(-\xi/\xi_c) + A_D \exp(+\xi/\xi_c)]^{-2}$ with $A_D > 0$, and $A_B + A_D = b_0^{-1/2}$.

We will next focus on the modeling of layers of *finite-thickness* with the profiles described in Eq. (32). Taking into account that these profiles reach b_0 and b_1, respectively, at the left edge ($\xi = 0$) and right edge ($\xi = \xi_1$) of the graded layer, they can also be expressed as follows:

$$b(\xi) = \left[b_0^{\pm 1/2} f(\xi_1 - \xi) + b_1^{\pm 1/2} f(\xi)\right]^{\pm 2} \quad ; \quad f(\xi) = \begin{cases} \sinh(\xi/\xi_c)/\sinh(\xi_1/\xi_c) & ; \quad \beta > 0 \\ \sin(\xi/\xi_c)/\sin(\xi_1/\xi_c) & ; \quad \beta < 0 \end{cases} \tag{33}$$

There is one degree of freedom left, namely the free parameter ξ_c, to adjust the shape of each profile. A possible objective is to reach a specific slope at the left boundary. This opens up many more opportunities, as compared to the linear profiles discussed in § 3.1. Consider again the case where effusivity triples from the left side to the right side: b_1/b_0 =3. Figure 16 shows a series of profiles of hyperbolic type, of either $\langle T \rangle$-form or $\langle \varphi \rangle$-form, and with varying left-edge slope. The same for trigonometric type profiles is shown in Fig. 17. In both cases, the set of $\langle T \rangle$-form profiles and the set of $\langle \varphi \rangle$-form profiles are limited by the corresponding "linear"-type profiles that share the same b_1/b_0 value (refer to the two profiles with $b_1/b_0 = 3$ in Fig. 3; their normalized derivative $\xi_1 b_0'/b_0$ is 1.464 for the $\langle T \rangle$-form profile and 0.845 for the $\langle \varphi \rangle$-form profile). In Fig. 16, the set of $\langle T \rangle$-form profiles extends from the corresponding "linear" limiting case downward and the set of $\langle \varphi \rangle$-form profiles extends from the corresponding "linear" limiting case upward. This makes the two sets present a recovery region for $\xi_1 b_0'/b_0 \in$ [0.845,1.464]. However, a $\langle T \rangle$-form profile and a $\langle \varphi \rangle$-form profile sharing the same value of the left derivative in this interval *are different*. In Fig. 17, the directions are reversed, creating an "empty" region between the two sets. This means that no profile of trigonometric type can be found in this intermediate region.

So, when the left-derivative target is greater than that of the $\langle T \rangle$-form curve of "linear-type" (here: 1.464), or smaller than that of the $\langle \varphi \rangle$-form curve of "linear-type" (here: 0.845), two distinct solutions can always be found: one of hyperbolic type and $\langle \varphi \rangle$-form, resp. $\langle T \rangle$-form (Fig. 16), and one of trigonometric type and $\langle T \rangle$-form, resp. $\langle \varphi \rangle$-form (Fig. 17) in the second case. If the left-derivative target is between these limiting values, there are, again, two solutions but of hyperbolic-type only (one of $\langle T \rangle$-form and one of $\langle \varphi \rangle$-form; see the recovery region in Fig. 16). In summary, given two end values b_0, b_1, and one value of the left-end derivative, b_0', there is always a possibility of choosing between two profiles in the joint class of trigonometric and hyperbolic profiles, of $\langle T \rangle$-form and $\langle \varphi \rangle$-form.

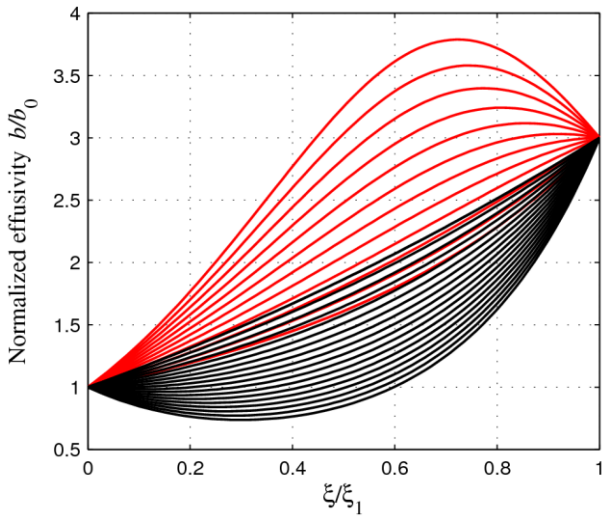

Fig. 16. Fundamental effusivity profiles of the *hyperbolic-type*. Same variables and normalizations as in Fig. 3. Profiles of $\langle T \rangle$-form are in black, those of $\langle \varphi \rangle$-form are in red. The right-to-left effusivity ratio b_1/b_0 is 3. For $\langle T \rangle$-form profiles, the (normalized) effusivity slope at the left edge takes on decreasing values starting from 1.464 in steps of 0.2. For $\langle \varphi \rangle$-form profiles, it takes on increasing values starting from 0.845. These values correspond to the slope values of the limiting "linear"-type profiles (see Fig. 3).

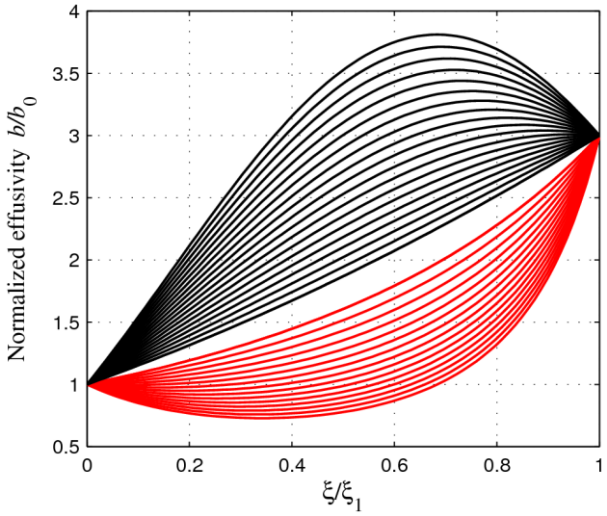

Fig. 17. Same as in Fig. 16 for the fundamental effusivity profiles of *trigonometric-type*. For $\langle T \rangle$-form profiles, the (normalized) effusivity slope at the left edge takes on increasing values starting from 1.464 in steps of 0.2. For $\langle \varphi \rangle$-form profiles, it takes on decreasing values starting from 0.845.

Previous illustrations have taken into account non-vanishing values of effusivity at the boundaries. The case in which effusivity is (asymptotically) null at one boundary, say $b_1 \to 0$, is also of interest. As was observed with the "linear"-type profile, only the $\langle T \rangle$-form profiles are then of practical interest. The hyperbolic and trigonometric solutions are illustrated in Fig. 18. The hyperbolic profiles all decrease monotonically, while the trigonometric profiles may also present other forms, such as, for example, with a rising portion first and then a falling portion.

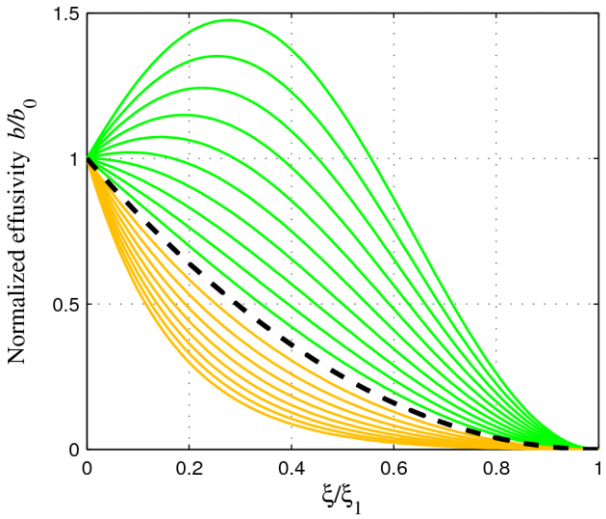

Fig. 18. Fundamental effusivity profiles of the "hyperbolic" type (in orange) and of the "trigonometric" type (in green) satisfying the boundary condition b_1=0. All are of $\langle T \rangle$-form. They extend on either side of a common limiting profile illustrated by a dashed black line, which corresponds to the "linear" type profile in Fig. 3 of the same line type. The (normalized) effusivity slope at the left edge takes on values from -2 to -6 ("hyperbolic" type) and from -2 to +3 ("trigonometric" type) in steps of 0.5.

3.2.2. Effusivity profiles in the z-space

Performing the inverse Liouville transformation is more involved than in the linear case. However, at least when VHC is constant ($q=0$), or heat conductivity is constant ($q=1$), closed-form analytical expressions describing the relationship between z and ξ can be found. First, the two coefficients A_B, A_D in Eq. (32) need to be evaluated from the edge values s_0, s_1 of the metaproperty $s(\xi)=b(\xi)^{\pm 1/2}$, namely:

$$\begin{cases} A_B = s_0 \\ A_D = \left(s_1 - s_0 B(\xi_1)\right)/D(\xi_1) \end{cases} \tag{34}$$

Next, we can take advantage of the fact that, for $q=0$ and $q=1$, the integral in Eq. (16) amounts to calculating the primitive of either $s^2(\xi)$ or $s^{-2}(\xi)$, which proves to be tractable [58], [61]:

$$g(\xi) \equiv \int_0^{\xi} s^2(u)du = \frac{\xi}{2}\left(A_B^2 - \operatorname{sign}(\beta)A_D^2\right) + \frac{\xi_c}{4}\left[\left(A_B^2 + \operatorname{sign}(\beta)A_D^2\right)D(2\xi) + 2\operatorname{sign}(\beta)A_B A_D\left(B(2\xi)-1\right)\right] \tag{35}$$

$$l(\xi) \equiv \int_0^{\xi} s^{-2}(u)du = \begin{cases} \dfrac{\xi_c}{A_D}\left(\dfrac{1}{s_0} - \dfrac{B(\xi)}{s(\xi)}\right) & \text{if} \quad A_D \neq 0 \\ \text{or} \quad \dfrac{\xi_c}{A_B}\dfrac{D(\xi)}{s(\xi)} & \text{if} \quad A_B \neq 0 \end{cases} \tag{36}$$

The choice between the primitives $g(\xi)$ or $l(\xi)$ for the z-scale determination depends on whether VHC is constant, i.e., $c(z)=c_0$, or conductivity is constant, i.e., $\lambda(z)=\lambda_0$, and on whether the profile is of $\langle T \rangle$-form or $\langle \varphi \rangle$-form. The selection rules are summarized thereafter:

$$\begin{aligned} &\text{if} \quad c(z)=cst=c_0 \quad \Rightarrow \begin{cases} \langle T\rangle: & z=g(\xi)/c_0 \\ \langle \varphi\rangle: & z=l(\xi)/c_0 \end{cases} \\ &\text{if} \quad \lambda(z)=cst=\lambda_0 \quad \Rightarrow \begin{cases} \langle T\rangle: & z=\lambda_0\, l(\xi) \\ \langle \varphi\rangle: & z=\lambda_0\, g(\xi) \end{cases} \end{aligned} \tag{37}$$

In addition, it is possible to eliminate the functions $B(\xi)$ and $D(\xi)$ in Eq. (36) by taking advantage of the fact that $B^2(\xi)-\text{sgn}(\beta)D^2(\xi)=1$. This leads to an explicit expression of the effusivity profile as a function of the physical depth z:

$$\left(\frac{1}{b^{\pm 1/2}(z)}\right)^2=\left(\frac{1}{b_0^{\pm 1/2}}+\frac{z}{z_1}\left(\frac{B(\xi_1)}{b_1^{\pm 1/2}}-\frac{1}{b_0^{\pm 1/2}}\right)\right)^2-\text{sgn}(\beta)\left(\frac{z}{z_1}\frac{D(\xi_1)}{b_1^{\pm 1/2}}\right)^2 \tag{38}$$

The right-hand side is a polynomial of degree two of the normalized depth z/z_1. Remember, however, that Eq. (38) concerns the cases requiring the calculation of the primitive $l(\xi)$. Hence, with reference to the rules provided in Eq. (37), the positive exponent in Eq. (38) applies to $\langle T\rangle$-form profiles with constant conductivity, whereas the negative exponent applies to $\langle \varphi\rangle$-form profiles with constant VHC. Depending on the form, the family of trigonometric and hyperbolic profiles (in terms of the metaproperty $s(\xi)$) takes on, in z-space, the form of a polynomial of degree 2 describing $1/b(z)$ or $b(z)$. This is a transposition in the thermal context of results obtained in electromagnetics in the modeling of a light wave at normal incidence in a material with a graded refractive index [64], [65], and later extended to the case of arbitrary incidence [61].

Figures 19 and 20 correspond to the profiles in Fig. 17 when represented in the physical-depth scale. To move from the SRDT-scale to the physical-depth scale it has been assumed that $c(z)=cst$ in Fig. 19 and that $\lambda(z)=cst$ in Fig. 20. The appropriate equations among Eq. (35)-(37), or possibly Eq. (38), have been considered to draw these plots.

When VHC is assumed constant, since from Eq. (14), $dz=b(\xi)c^{-1}(\xi)d\xi$, it is clear that moving from $b(\xi)$ to $b(z)$ induces a horizontal stretching/compression of the profile in those areas where effusivity is the highest/lowest (compare Figs. 17 and 19). Conversely, when conductivity is assumed to be constant, since from Eq. (14), $dz=\lambda(\xi)b^{-1}(\xi)d\xi$, moving from $b(\xi)$ to $b(z)$ induces the opposite (compare Figs. 17 and 20).

The same has been performed with the hyperbolic–type profiles from Fig. 16 (not reproduced here due to lack of space). Naturally, the same stretching/compression effects have been observed with these profiles.

For hypotheses regarding a, c or λ other than being constant, to establish a relationship between the ξ-scale and the z-scale would probably require the numerical computation of a quadrature. The quadrature in question is that in Eq. (16), if $\lambda^q(z)c^{q-1}(z)$ happens to be constant, or one among those in Eq. (13), if one of the following profiles is known: $a(z)$, $c(z)$ or $\lambda(z)$.

In any case, Figs. 16 to 20 show that implementing the family of trigonometric and hyperbolic profiles quite substantially enriches the possibilities, as compared to the simple "linear"-type profiles. In essence, one additional free parameter is made available to play with the concavity of the profile and possibly introduce a change of sign to the concavity.

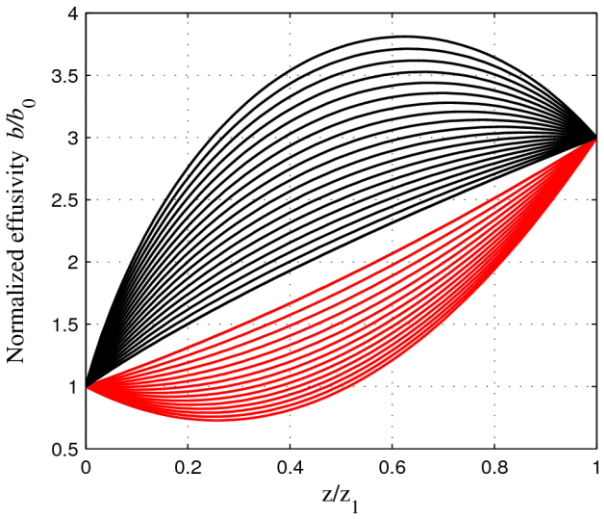

Fig. 19. *Trigonometric*-type profiles from Fig. 17 expressed here in terms of the normalized geometrical depth z/z_1. To perform the inverse Liouville transformation in Eq. (15), *the volumetric heat capacity* has been assumed to be *constant*.

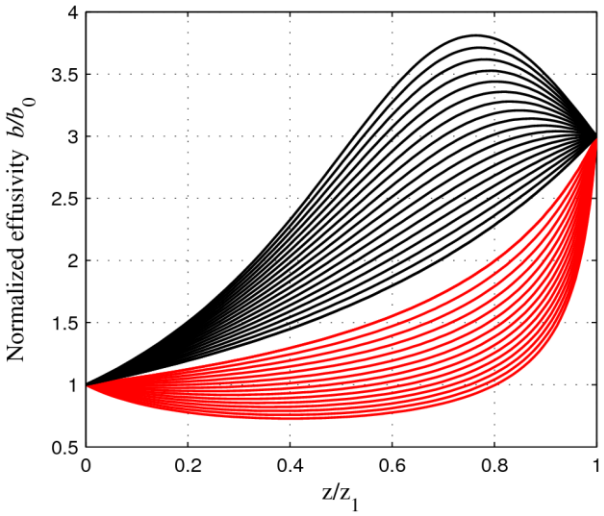

Fig. 20. Same as in Fig. 19 when assuming that the *thermal conductivity* is *constant*.

3.2.3. Quadrupole related to hyperbolic and trigonometric profiles

Regarding the field function $\psi(\xi,p)$, the only difference with the linear case, is that $\sqrt{p}$ is now replaced by $\sqrt{p+\beta}$:

$$\psi(\xi,p) \propto \begin{bmatrix} K(\xi,p) \\ P(\xi,p) \end{bmatrix} \equiv \begin{bmatrix} C^{(\beta)}(\xi) \\ S^{(\beta)}(\xi) \end{bmatrix} \quad ; \quad \begin{bmatrix} C^{(\beta)}(\xi) \\ S^{(\beta)}(\xi) \end{bmatrix} \equiv \begin{bmatrix} \cosh\left(\sqrt{p+\beta}\xi\right) \\ \sinh\left(\sqrt{p+\beta}\xi\right) \end{bmatrix} \tag{39}$$

The entries of the corresponding quadrupole are obtained after some algebra:

$$\begin{bmatrix} A \\ B \\ C \\ D \end{bmatrix} = \begin{bmatrix} x \\ \xi_1/(s_0 s_1) \\ s_0 s_1/\xi_1 \\ x^{-1} \end{bmatrix} \bullet \left(\begin{bmatrix} 1 & -\chi_1 \\ 0 & 1 \\ \chi_0 - \chi_1 & (p+\beta)\xi_1^{\,2} - \chi_0\chi_1 \\ 1 & \chi_0 \end{bmatrix} \times \begin{bmatrix} \cosh\left(\sqrt{p+\beta}\,\xi_1\right) \\ \dfrac{1}{\sqrt{p+\beta}\,\xi_1} \sinh\left(\sqrt{p+\beta}\,\xi_1\right) \end{bmatrix} \right) \quad ; \quad \begin{cases} x \equiv \dfrac{s_1}{s_0} \\ \chi_{0,1} \equiv \dfrac{\xi_1 s'_{0,1}}{s_{0,1}} \end{cases} \tag{40}$$

From the profile definition, it is easy to obtain the expressions of the normalized logarithmic derivatives at the layer boundaries, χ_0 and χ_1, which appear in Eq. (40) :

$$\begin{bmatrix} \chi_0 \\ \chi_1 \end{bmatrix} = \frac{\xi_1}{\xi_c D(\xi_1)} \begin{bmatrix} x - B(\xi_1) \\ B(\xi_1) - x^{-1} \end{bmatrix} \quad ; \quad x = \frac{s_1}{s_0} \tag{41}$$

Again, to obtain the quadrupole matrix $\mathbf{M}_{\langle T \rangle}$ related to a $\langle T \rangle$-form profile, one simply has to make the substitution $s_{0,1} \leftarrow b_{0,1}^{\,+1/2}$ in Eqs. (40) and (41), whereas for the quadrupole matrix $\mathbf{M}_{\langle \varphi \rangle}$ related to a $\langle \varphi \rangle$-form profile, one should first make the substitution $s_{0,1} \leftarrow b_{0,1}^{\,-1/2}$ and then apply the permutation rule described in Eq. (A-6).

3.2.4. Temperature computations

The temperature has been computed to simulate the same modulated photothermal experiment as that considered with the "linear"-type coatings in § 3.1.4. For that purpose, the quadrupole entries defined in Eq. (40) have been substituted in the temperature expression in Eq. (29).

The following illustrations refer again to the case where effusivity triples from the free surface of the coating down to the interface with the substrate: $b_1/b_0 = 3$.

The results obtained with the hyperbolic-type profiles drawn in Fig. 16 are plotted in Figs. 21-22. The results obtained with the trigonometric-type profiles drawn in Fig. 17 are plotted in Figs. 23-24. The amplitude response $|\theta_0|$ has been reported only through the inverse contrast $|\theta_0^{ref}|/|\theta_0|$ (Figs. 22 and 24), which, as has already been explained above, represents the normalized *apparent effusivity* (in the frequency domain).

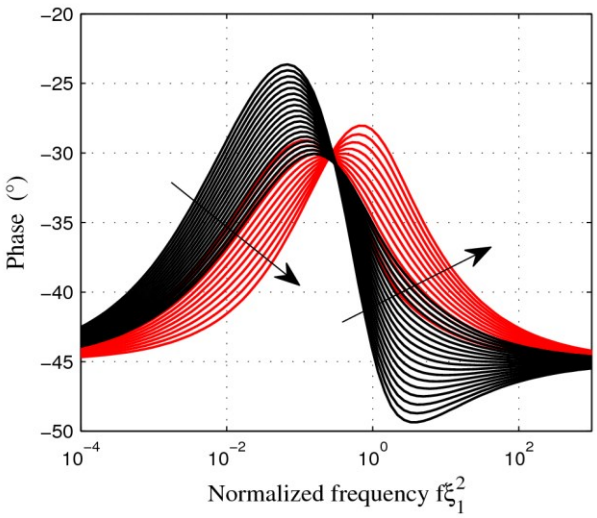

Fig. 21. Thermal periodic response (*phase* of the surface temperature) of coating/substrate bilayers with coatings of *hyperbolic-type*. The corresponding profiles are represented in Fig. 16 (with the same colors). The arrows indicate an increasing slope of the effusivity profile at the free surface ($z = \xi$ =0).

Let us recall that the temperature amplitude evolves with a frequency according to the general rule: effusivity at a small/large depth is anti-correlated with the amplitude at a high/low frequency. However, this effect is progressively dampened with depth. In addition, local features in the effusivity profile are sensed over a frequency range that widens (in a logarithmic scale) as the depth increases. As a consequence, the shallow effusivity features are more clearly revealed in the apparent effusivity curve than the deeper features (see Fig. 22 and Fig. 24). Clear evidence is obtained when considering the overshoot that some of the effusivity profiles present, as compared to the final level b_1/b_0 =3. This is observed for the highest red profiles in Fig. 16 and the highest black profiles in Fig. 17. Such an overshoot is, however, not seen in the related curves of the apparent effusivity in Figs. 22 and 24: the apparent effusivity does not exceed the asymptotic level of 3 when the frequency is decreasing. This poor restitution of the actual in-depth evolution of effusivity explains the difficulty encountered in achieving a thermal inversion of deep features with great precision.

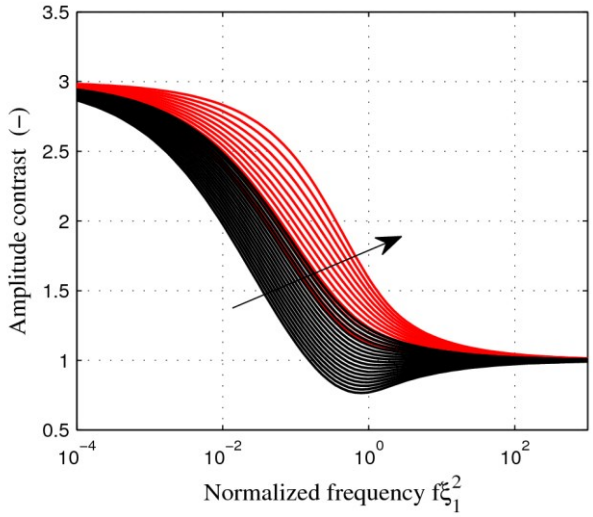

Fig. 22. Same as in Fig. 21 for the amplitude inverse contrast (i.e., the apparent effusivity in the frequency domain).

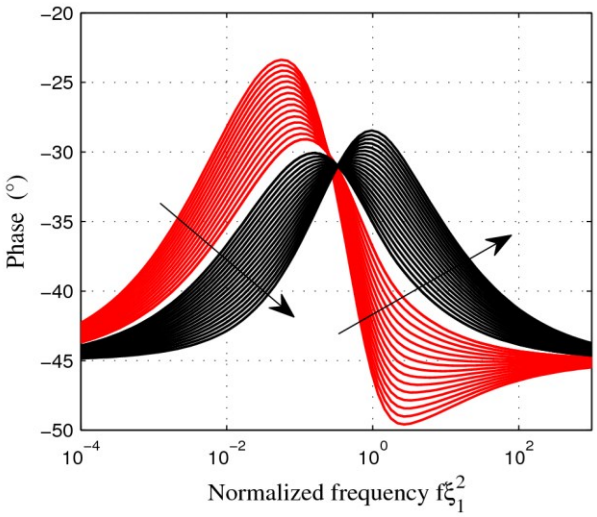

Fig. 23. Thermal periodic response (*phase*) of coating/substrate bilayers with coatings of *trigonometric-type*. The corresponding profiles are represented in Fig. 17 (with the same colors). The arrow indicates an increasing slope of the effusivity profile at the free surface.

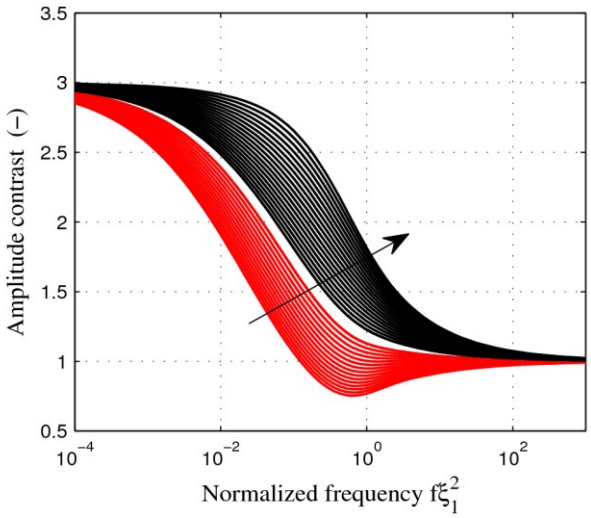

Fig. 24. Same as in Fig. 23 for the amplitude inverse contrast (i.e. the apparent effusivity in the frequency domain).

Let us now analyze the thermal response of hyperbolic and trigonometric profiles in the two limiting cases $b_1 \to 0$ ($\langle T \rangle$-form), and $b_1 \to \infty$ ($\langle \varphi \rangle$-form). The expression in Eq. (29) reduces to:

$$\theta_0 = \frac{\wp}{b_0\sqrt{p}}\left[\frac{\sqrt{p}\xi_1}{\sqrt{p+\beta}\xi_1 \coth\left(\sqrt{p+\beta}\xi_1\right)+\chi_0+h\xi_1 b_0^{-1}}\right] \quad ; \quad b_1 \to 0 \tag{42}$$

$$\theta_0 = \frac{\wp}{b_0\sqrt{p}}\left[\frac{\sqrt{p}\xi_1}{\sqrt{p+\beta}\xi_1 \coth\left(\sqrt{p+\beta}\xi_1\right)+\chi_0}+\frac{h}{b_0\sqrt{p}}\right]^{-1} \quad ; \quad b_1 \to \infty \tag{43}$$

The expressions in Eq. (42) and Eq. (43) encompass the "linear" case, which was described respectively in Eq. (30) and Eq. (31). As a matter of fact, in the linear case we have $\beta = 0$ and $\chi_0 = -1$.

The following two figures concern only the first case, $b_1 \to 0$ ($\langle T \rangle$-form). The phase of the periodic response is shown in Fig. 25, while the inverse contrast in amplitude is shown in Fig. 26.

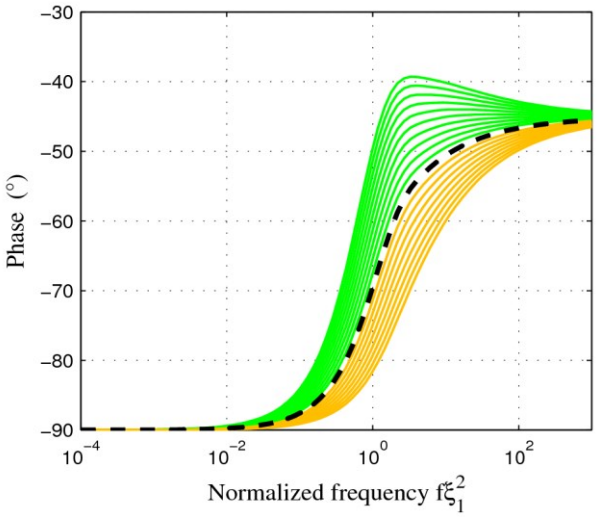

Fig. 25. Phase of the modulated temperature response of the graded layers represented in Fig. 18 (same colors).

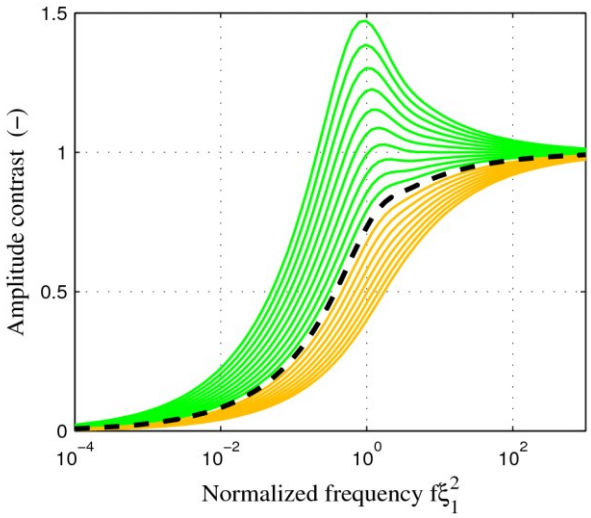

Fig. 26. Same as in Fig. 25 for the amplitude inverse contrast (i.e., the apparent effusivity in the frequency domain).

As compared to the response of the "linear"-type graded layer, the variations of effusivity introduced through the hyperbolic or trigonometric character of the new profiles induce significant changes in phase and amplitude in a frequency range of the order of $f\xi_1^2 \in [0.1,10]$, especially around $f\xi_1^2 \approx 1$.
These examples complete the description of the possibilities offered by the hyperbolic and trigonometric types of effusivity profiles.

4. Discussion and conclusion

An in-depth analysis was carried out on three classes of effusivity profiles expressed in the Liouville space (i.e., versus the square root of the integrated diffusion time ξ), the so-called "linear", "trigonometric" and "hyperbolic" profiles. These mathematical functions actually describe the metaproperty $s(\xi)$, which represents either the square root of effusivity ($\langle T \rangle$-form profiles) or its inverse ($\langle \varphi \rangle$-form profiles). They have in common that they lead to very simple analytical solutions for the dynamic temperature in the Laplace or Fourier domain. Furthermore, the quadrupole of a planar slab whose effusivity shows either type of these profiles has been provided. These quadrupoles are probably the simplest ones related to graded materials. Therein, the classical hyperbolic functions of $\sqrt{p}\xi$ needed to model homogeneous slabs are complemented by rational functions of $\sqrt{p}\xi$ of degree 2 at most for the numerator, and degree 1 at most for the denominator (in the hyperbolic and trigonometric cases $\sqrt{p}\xi$ is replaced by $\sqrt{p+\beta}\xi$). The important result is that the temperature and flux expressions involve no special functions, contrarily to the vast majority of graded-profile solutions found in the literature.
Each solvable profile $b(\xi)$ yields a multiplicity of thermal-property representations in the physical-depth space, as was shown for all three classes. This perfectly highlights the leverage effect of the Liouville transformation in finding solvable profiles. The related inverse Liouville transformation $\xi \to z$ is fueled by independent information on the distribution of one from among the other thermal properties, or a combination thereof, which boosts the number of solvable profiles.
Single layers with "linear", "trigonometric" or "hyperbolic" effusivity profiles have been considered to model the photothermal response (either modulated or pulsed) of graded coatings deposited on a homogeneous substrate. Numerous parametric plots describing the phase of the front surface temperature vs. frequency, its amplitude and the so-called *apparent effusivity* have been provided (the apparent effusivity has also been provided vs. time as a description of the transient response to a pulse heating). The chosen presentation with non-dimensional parameters is intended to easily translate the results into a wide range of

applications. The extension to other combinations of parameters is left to the reader, which is a very easy task, because of the simple expressions of the quadrupoles.

These quadrupoles could then be assembled to model a stacking of graded layers, each of them having its own SRDT. Let us now compare different versions of 1D multilayer quadrupole models. All provide the exact thermal response at any external surface and any interface, both in the periodic or transient regime. In the classical piece-wise constant effusivity model [30], [55], effusivity is discontinuous; the model will be considered of level 0. It introduces one adjustable parameter (namely the assigned effusivity value) for each of the N considered layers. A model made of "linear"-type layers will be considered of level 1 since the effusivity profile can be made continuous at the interfaces. A system where M "linear"-type layers are stitched so that there is no discontinuity at the nodes would introduce M+1 parameters, namely the effusivity at the nodes. Let us recall that the linearity is with respect to the metaproperty $s(\xi)$, which means either $b^{1/2}(\xi)$ or $b^{-1/2}(\xi)$. This choice is open for each layer, which gives 2^M possibilities. Of course, for the same quality of fit with respect to a given real profile (as measured, for example, through least-squares), it will be possible to select a number of graded layers M much smaller than N. Then, a model made of "hyperbolic"-type or "trigonometric"-type layers will be considered of level 2 since not only the effusivity profile can be made continuous at the interfaces, but there is one additional free parameter to adjust the slope at one or the other edge of each layer. A stacking of K "hyperbolic"-type or "trigonometric"-type layers with a continuous effusivity is thus described with 2K+1 parameters (with again 2^K possibilities regarding the $\langle T \rangle$-form or $\langle \varphi \rangle$-form choice). The additional intrinsic parameters will allow playing on the curvature of each individual profile. Again, this will open up the possibility of reducing the number of layers, without compromising the accuracy of the fit. This reduction should be placed in balance with the increased number of parameters needed to define each layer in the selection of the best compromise, which is certainly situation-dependent. In any case, the simplicity of the quadrupoles of the "hyperbolic"-type or "trigonometric"-type layers contributes to relaxing the compromise.

Yet, one degree of freedom is lacking to adjust independently both end-slopes in each layer. Such flexibility is actually reached with the so-called $\mathrm{sech}(\hat{\xi})$-type profiles which are based on four adjustable parameters [58]. However, their quadrupole (see Ref. [60]) is somewhat more complicated (although it is still based on elementary functions only) than those described in the present paper.

In the end, the new analytical tools exposed here would allow approaching the thermal response of a real (graded) material with less quadrupoles than with the classical level-0 method. The performance regarding flexibility is not as high as with more sophisticated profiles like the $\mathrm{sech}(\hat{\xi})$-type profiles, but the computational cost is lower. One should still stress that the parameter ξ_c in the "hyperbolic"-type or "trigonometric"-type profiles is a *non-linear* parameter. Whatever the additional constraint on the profile shape (e.g. left or right derivative), the determination of the value of ξ_c requires using a non-linear solver. This is not the case for the "linear"-type profiles for which both parameters are simply linear. This aspect should be taken into consideration when choosing between level-1 and level-2 models (notice that quadrupoles of different levels could be mixed in a multilayer).

The applications of the analytical tools presented here concern the modeling of thermal behavior in-service or the off-line characterization of a wide variety of materials in which the thermal properties show a gradation that is essentially one-dimensional. This concerns typically functionally graded materials (FGM) with graded coatings (e.g. ceramic thermal barrier coatings for turbine blades, aerospace structures or fusion reactors, ceramic/metal FGMs) or materials with a shallow transformation (e.g. case-hardened steel). Other examples are fiber-reinforced composites where the concentration of fibers changes with depth (e.g. injection-molded thermoplastics or thermosets with short metallic of carbon fibers). An example from the environment realm is the thermal modeling of soils where the graded structure is of geologic origin or it is induced by differences in water concentration.

The described method deals with the 1D heat equation. Extensions to 2D or 3D problems can be considered in the context of the application of the well-known method of separation of variables. This means that the case of anisotropic plates could be considered, i.e. with conductivity in the z direction $\lambda_z(z)$, conductivity in the x direction $\lambda_x(x)$ and conductivity in the y direction $\lambda_y(y)$. Some indications have already been given in [58] for the 2D case (the extension to 3D would be straightforward). It was shown that after a separation of

variables, and provided that volumetric heat capacity is constant, the heat equation in the Liouville space is reduced to the same form as in the 1D case. The problem is then formally solved. Nevertheless, one should be aware that the global solution then expresses through a series (or two imbedded series, in 3D) involving the eigenfunctions relative to the transverse direction x (or x and y in 3D).

The solvable profiles discussed in this paper, and more precisely the corresponding functions describing the metaproperty $s(\xi)$, have already found applications in areas other than thermal diffusion. As a matter of fact, graded layers with a linear, trigonometric or hyperbolic evolution of the function $s(\xi)$ have been considered for the electromagnetic-wave problem in [61], [64] and [65]. Let us recall that the admittance and refractive index profiles (in a normalized form) can be described with the same functions that have been used here for effusivity (see, e.g., Fig. 3 and Figs. 16-17). The counterparts of the $\langle T \rangle$-form and $\langle \varphi \rangle$-form profiles have been called the $\langle E \rangle$-form and $\langle H \rangle$-form profiles ($\langle E \rangle$ for "electric" and $\langle H \rangle$ for "magnetic"). A quite remarkable result is that the reflectance spectra of the two forms of profiles are *exactly the same* (provided that the electromagnetic admittance is continuous at both edges of the graded coating) [61]. Conversely, with regard to heat diffusion, it is impossible for two distinct $\langle T \rangle$-form and $\langle \varphi \rangle$-form profiles to give the same (thermal) response at any frequency.

Other fields of application for the solvable profiles discussed in this paper can be found among those cited in [58]: (i) mass diffusion (2nd Fick's law) in structures presenting a variable diffusion coefficient, (ii) 1st and 2nd Stokes problems in fluids with variable viscosity, (iii) advection-diffusion related to pollutant dispersion in a turbulent atmosphere where the wind speed and the eddy diffusivity depend on the height above the ground surface, and (iv) tapered RC transmission lines. In addition to these, we can mention: (i) the Graetz problem with an arbitrary profile of the fluid velocity in the boundary layer, and (ii) thin fins with either variable conductivity or variable thickness and possibly a variable heat coefficient.

The application of the present tools to these problems will present varying degrees of difficulty. Nevertheless, note that the seemingly exotic case of a graded layer presenting a vanishing effusivity at one boundary (see Fig. 3, 12-15, 18, 25-26) may be well suited to model advection-diffusion in laminar or turbulent boundary layers, since the parameter that corresponds to effusivity in thermal diffusion actually vanishes in the vicinity of the solid surface. The transposition to the previous problems of the tools presented in this paper is now underway, as well as their implementation to solve related inversion problems.

APPENDIX

A set of useful relations between the effusivity profiles of $b(\xi)$ and the metaproperty $s(\xi)$ on one side and between the thermal fields $\theta(\xi,p)$, $\phi(\xi,p)$ and $\psi(\xi,p)$ on the other side, for either $\langle T \rangle$-form profiles or $\langle \varphi \rangle$-form profiles is first recalled [58]:

$$\langle T \rangle : \begin{cases} b = s^2 \\ \theta = \psi\, s^{-1} \\ \phi = -W(s,\psi) \end{cases} \qquad \langle \varphi \rangle : \begin{cases} b = s^{-2} \\ \theta = -p^{-1} W(s,\psi) \\ \phi = \psi\, s^{-1} \end{cases} \tag{A-1}$$

where W is the Wronskian: $W(s,\psi) = s\psi' - s'\psi$.

The quadrupole (or transfer) matrix $\mathbf{M}$ of a layer extending from $z = z_0$ to $z = z_1$ (i.e., from $\xi = \xi_0$ to $\xi = \xi_1$ in the Liouville space; in the sequel, the indexes 0 and 1 mean that the variable under study is evaluated, respectively, at ξ_0 and at ξ_1) relates the input temperature/heat flux vector, i.e., $[\theta_0 \quad \phi_0]^t$, to the output vector, i.e., $[\theta_1 \quad \phi_1]^t$, as follows (see, e.g., [58]):

$$\begin{bmatrix} \theta_0 \\ \phi_0 \end{bmatrix} = \mathbf{M} \cdot \begin{bmatrix} \theta_1 \\ \phi_1 \end{bmatrix} \quad ; \quad \begin{cases} \langle T \rangle : & \mathbf{M} \equiv \mathbf{M}_{\langle T \rangle} \\ \langle \varphi \rangle : & \mathbf{M} \equiv \mathbf{M}_{\langle \varphi \rangle} \end{cases} \tag{A-2}$$

The calculation of the quadrupole $\mathbf{M}_{\langle T\rangle}$ follows the classical procedure described, for instance, in [33], [55], and [56]. Hence, a synthetic expression for $\mathbf{M}_{\langle T\rangle}$ is given by:

$$\mathbf{M}_{\langle T\rangle} = \begin{bmatrix} K/s & P/s \\ -W(s,K) & -W(s,P) \end{bmatrix}_0 \times \begin{bmatrix} K/s & P/s \\ -W(s,K) & -W(s,P) \end{bmatrix}_1^{-1} \tag{A-3}$$

After some algebra, the four entries of the matrix are expressed as follows:

$$\mathbf{M}_{\langle T\rangle} \equiv \begin{bmatrix} A & B \\ C & D \end{bmatrix} = \frac{1}{\Delta}\begin{bmatrix} (s_1 G - s_1' I)/s_0 & I/(s_0 s_1) \\ s_0' s_1 G + s_0 s_1' H - s_0' s_1' I - s_0 s_1 J & (s_0' I - s_0 H)/s_1 \end{bmatrix} \tag{A-4}$$

The terms G, H, I, J, Δ involve the values taken at the two layer edges by the independent functions $K(\xi, p)$ and $P(\xi, p)$ and by their derivatives:

$$\begin{cases} G = K_0 P_1' - K_1' P_0 & H = K_0' P_1 - K_1 P_0' \\ I = K_0 P_1 - K_1 P_0 & J = K_0' P_1' - K_1' P_0' \\ \Delta = K_1 P_1' - K_1' P_1 = K_0 P_0' - K_0' P_0 \end{cases} \tag{A-5}$$

In Eq. (A-4), the boundary values of the metaproperty $s(\xi)$, namely s_0, s_1, s_0', s_1' are obtained from the boundary values of the effusivity, b_0, b_1, b_0' and b_1' according to: $s_{0,1} = b_{0,1}^{+1/2}$ and $s_{0,1}' = b_{0,1}'/\left(2b_{0,1}^{1/2}\right)$.

The quadrupole matrix $\mathbf{M}_{\langle\varphi\rangle}$ deserves a special treatment as described in [58] and [60]. It is obtained by first calculating the four entries *A, B, C, D* defined in Eq. (A-4), by substituting into the boundary values s_0, s_1, s_0', s_1' those obtained from the boundary specifications b_0, b_1, b_0' and b_1' *when considering the specific* $\langle\varphi\rangle$ *-form profile*. This means that $s_{0,1} = b_{0,1}^{-1/2}$ and $s_{0,1}' = -b_{0,1}'/\left(2b_{0,1}^{3/2}\right)$. The final step is to perform the pseudo-permutation:

$$\mathbf{M}_{\langle\varphi\rangle} = \begin{bmatrix} D & p^{-1}C \\ pB & A \end{bmatrix} \tag{A-6}$$

REFERENCES

[1] Khor K.A., Gu Y.W., "Thermal properties of plasma-sprayed functionally graded thermal barrier coatings," Thin Solid Films, 372, pp. 104-113, (2000).

[2] V. Birman, L.W. Byrd, "Modeling and analysis of functionally graded materials and structures," Appl. Mech. Rev., 60, pp. 195-216, (2007).

[3] Carpio P., Salvador M. D., Borrell A., Sánchez E. "Thermal behaviour of multilayer and functionally-graded YSZ/Gd2Zr2O7 coatings," Ceram. Int., 43(5), 4048-4054, (2017).

[4] Lan T.T.N., Seidel U., Walther H.G., Goch G., Schmitz B., "Experimental results of photothermal microstructural depth profiling," J. Appl. Phys., 77, 4108-4111, (1995).

[5] Munidasa M., Funak F., Mandelis A., "Application of a generalized methodology for quantitative thermal diffusivity depth profile reconstruction in manufactured inhomogeneous steel-based materials," J. Appl. Phys., 83, pp. 3495-3498, (1998).

[6] Krapez J.-C., "Thermal effusivity profile characterization from pulse photothermal data," J. Appl. Phys., 87, pp. 4514-4524, (2000).

[7] Walther H.G., Fournier D., Krapez J.-C., Luukkala M., Schmitz B., Sibilia C., Stamm H., Thoen J., "Photothermal Steel Hardness Measurements - Results and Perspectives," Anal. Sci., 17, pp. 165-168, (2001).

[8] Krapez J.-C., Li Voti R., "Effusivity depth profiling from pulsed radiometry data: comparison of different reconstruction algorithms," Anal. Sci., 17, pp. 417-418, (2001).

[9] Nagasaka Y., Sato T., Ushiku T., "Non-destructive evaluation of thermal diffusivity distributions of functionally graded materials by photothermal radiometry," Meas. Sci. Techn., 12, pp. 2081-2088, (2001)

[10] Qu H., Wang C., Guo X., Mandelis A., "Reconstruction of depth profiles of thermal conductivity of case hardened steels using a three-dimensional photothermal technique," J. Appl. Phys., 104, pp. 113518, (2008).

[11] Celorrio R., Apiñaniz E., Mendioroz A., Salazar A., Mandelis A. "Accurate reconstruction of the thermal conductivity depth profile in case hardened steel," J. Appl. Phys., 107(8), 083519, (2010).

[12] Apiñaniz E., Mendioroz A., Salazar A., Celorrio R., "Analysis of the Tikhonov regularization to retrieve thermal conductivity depth-profiles from infrared thermography data," J. Appl. Phys., 108, pp. 064905, (2010).

[13] Fivez J., Glorieux C., "Case hardening inspection of steel using photothermal phase maxima," J. Appl. Phys., 108, pp. 103506, (2010).

[14] Archiopoli U.C., Mingolo N., Martínez O.E., "Two-dimensional mapping of micro-hardness increase on surface treated steel determined by photothermal deflection microscopy," Surface Coatings Tech., 205, pp. 3087–3092, (2011).
[15] Li Voti R. L., Leahu G., Sibilia C, "A New Device for High-Accuracy Measurements of the Hardness Depth Profile in Steels," In Proceedings of 4th International Conference in Software Engineering for Defence Applications (pp. 239-242). Springer, Cham. (2016).
[16] Jeon R.J., Mandelis A., Abrams S.H., "Depth profilometric case studies in caries diagnostics of human teeth using modulated laser radiometry and luminescence," Rev. Sci. Instrum., 74, pp. 380-383, (2003).
[17] Martinez-Torres P., Mandelis A., Alvarado-Gil J.J., "Photothermal determination of thermal diffusivity and polymerization depth profiles of polymerized dental resins," J. Appl. Phys., 106, pp. 114906, (2009).
[18] Martinez-Torres P., Mandelis A., Alvarado-Gil J.J., "Optical and thermal depth profile reconstructions of inhomogeneous polymerization in dental resins using photothermal waves," J. Appl. Phys., 108, pp. 054902, (2010).
[19] Cotta R.M., Cotta B.P., Naveira-Cotta C.P., Cotta Pereira G., "Hybrid integral transforms analysis of the bioheat equation with variable properties," Int. J. Thermal Sci., 49, pp. 1510-1516, (2010).
[20] Sutradhar A., Paulino G. H., "The simple boundary element method for transient heat conduction in functionally graded materials," Comput. Meth. Appl. Mech. Engrg., 193,pp. 4511–4539, (2004).
[21] Wang, H., Qin, Q. H., & Kang, Y. L. "A meshless model for transient heat conduction in functionally graded material," Computational mechanics, 38(1), 51-60, (2006).
[22] Reutskiy, S. Y. "A meshless radial basis function method for 2D steady-state heat conduction problems in anisotropic and inhomogeneous media," Engineering Analysis with Boundary Elements, 66, 1-11, (2016).
[23] Lin, J., Reutskiy, S. Y., & Lu, J. "A novel meshless method for fully nonlinear advection–diffusion-reaction problems to model transfer in anisotropic media," Applied Mathematics and Computation, 339, 459-476, (2018).
[24] Liu, P., Yu, T., Bui, T. Q., Zhang, C., Xu, Y., & Lim, C. W. "Transient thermal shock fracture analysis of functionally graded piezoelectric materials by the extended finite element method," International journal of solids and structures, 51(11-12), 2167-2182, (2014).
[25] Yu, T., Bui, T. Q., Yin, S., Doan, D. H., Wu, C. T., Van Do, T., & Tanaka, S. "On the thermal buckling analysis of functionally graded plates with internal defects using extended isogeometric analysis," Composite Structures, 136, 684-695, (2016).
[26] Naveira-Cotta C.P., Cotta R.M., Orlande H.R.B., Fudym O., "Eigenfunction expansions for transient diffusion in heterogeneous media," Int. J. Heat Mass Transf., 52, pp. 5029-5039, (2009).
[27] Naveira-Cotta C.P., Cotta R.M., Orlande H.R.B., "Inverse analysis with integral transformed temperature fields: Identification of thermophysical properties in heterogeneous media," Int. J. Heat Mass Transf., 54, pp. 1506-1519, (2011).
[28] Naveira-Cotta C.P., Orlande H.R.B., Cotta R.M., "Combining Integral Transforms and Bayesian Inference in the Simultaneous Identification of Variable Thermal Conductivity and Thermal Capacity in Heterogeneous Media," J. Heat Transf., 133, pp. 111301, (2011).
[29] Khmelnytskaya K.V., Serroukh I., "The heat transfer problem for inhomogeneous materials in photoacoustic applications and spectral parameter power series," Math. Meth. Appl. Sci., 11, pp. 065707, (2013).
[30] Carslaw H.S., Jaeger J.C., *Conduction of heat in solids*, Oxford Univ. Press, pp. 15.412-15.415, (1959).
[31] Novak M. D. "Theoretical values of daily atmospheric and soil thermal admittances," Boundary-Layer Meteorology, 34(1-2), 17-34, (1986).
[32] Massman W.J., "Periodic temperature variations in an inhomogeneous soil: a comparison of approximate and exact analytical expressions," Soil Sci., 155, pp. 331-338, (1993).
[33] Sengupta, A., Sodha, M. S., Verma, M. P., Sawhney, R. L., & Asthana, M. "Periodic heat transfer through inhomogeneous media. Part 1. Slab," Int. J. Ener. Res, 16(9), pp. 787-802, (1992).
[34] Thakur A.K.S., "Periodic heat transfer through an inhomogeneous medium," Lett. Heat Mass Transfer, 9, pp. 385-394, (1982).
[35] Sodha M.S., Sengupta A., Sawhney R.L., "Use of linear profile layers for the evaluation of the admittance matrix of an inhomogeneous slab," Int. J. Ener. Res., 17, pp. 121-125, (1993).
[36] Fivez, J., Thoen, J. "Thermal waves in materials with linearly inhomogeneous thermal conductivity," Journal of applied physics, 75(12), 7696-7699, (1994).
[37] Glorieux C., Bozoki Z., Fivez J., Thoen J., "Photoacoustic depth profiling of the thermal conductivity of an inhomogeneously aligned liquid crystal at a free surface," J. Appl. Phys., 78, pp. 3096-3101, (1995).
[38] Lan T.T.N., Seidel U., Walther H.G., "Theory of microstructural depth profiling by photothermal measurements," J. Appl. Phys., 77, pp. 4739-4745, (1995).
[39] Karam M.A., "A thermal wave approach for heat transfer in a nonuniform soil," Soil Sci. Soc. Am. J., 64, pp. 1219–1225, (2000).
[40] Friedrich K., Seidel U., Walther H. G., Karpen W., & Busse G. "Proposal for photothermal characterization of boundaries between layer and substrate," Research in Nondestructive Evaluation, 5(1), 31-39, (1993).
[41] Cossali G.E., "Dynamic response of a non homogeneous 1D slab under periodic thermal excitation," Int. J. Heat Mass Transf., 50 pp. 3943-3948, (2007).
[42] Hosseini S. M., Akhlaghi, M., Shakeri, M. "Transient heat conduction in functionally graded thick hollow cylinders by analytical method," Heat and Mass Transfer, 43(7), 669-675, (2007).
[43] Sutton O. G. "Wind structure and evaporation in a turbulent atmosphere," Proc. R. Soc. Lond. A, 146, pp. 701-722, (1934).
[44] Bosanquet C. H., Pearson J. L. "The spread of smoke and gases from chimneys," Trans. Faraday Soc., 32, pp. 1249-1263, (1936).
[45] Sutton, W. G. L. "On the equation of diffusion in a turbulent medium," Proc. R. Soc. Lond. A, 182, pp. 48-75, (1943).
[46] Jaeger J. C. "Diffusion in turbulent flow between parallel planes," Quart. Appl. Math., 3, pp. 210-217, (1945).
[47] Calder K. L. "Eddy diffusion and evaporation in flow over aerodynamically smooth and rough surfaces: a treatment based on laboratory laws of turbulent flow with special reference to conditions in the lower atmosphere," Quart. J. of Mech. Appl. Math., 2, pp. 153-176, (1949).

[48] Smith F. B., "The diffusion of smoke from a continuous elevated point-source into a turbulent atmosphere," J. of Fluid Mech., 2, pp. 49-76, (1957).
[49] Zhou Y.T., Lee K.Y., Yu D.H., "Transient heat conduction in a functionally graded strip in contact with well stirred fluid with an outside heat source," Int. J. Heat Mass Transf. 54, 5438-5443 (2011).-
[50] Fivez J., Thoen J., "Thermal waves in materials with inhomogeneous thermal conductivity: an analytical approach," J. Appl. Phys., 79, pp. 2225-2228, (1996).
[51] Zhao, J., Ai, X., Li, Y. Z. "Transient temperature fields in functionally graded materials with different shapes under convective boundary conditions," Heat Mass Transf., 43(12), 1227-1232 (2007).
[52] Ishiguro T., Makino A., Araki N., Noda N., "Transient Temperature Response in Functionally Gradient Materials," Int. J. Thermophys., 14, pp. 101-121, (1993).
[53] Krapez J.-C., Profice S., "Quadripôles pour l'étude de la diffusion dans les matériaux à profils de propriétés continus. Application aux transferts couplés thermique/ hydrique dans les sols non saturés," Proc. SFT 2011, http://www.sft.asso.fr/Local/sft/dir/user-3775/documents /actes/congres_2011/Communications/134.pdf, (2011).
[54] Alvarado-Leaños J. J., Ordonez-Miranda J., Alvarado-Gil J. J., "Thermal Resistance Formulation of Fourier Equation and Its Application in the Study of Inhomogeneous Materials and Inverse Problems," Int. J. Thermophys., 34, pp. 1457-1465, (2013).
[55] Maillet D., André S., Batsale J.-C., Degiovanni A., Moyne C., *Thermal Quadrupoles: Solving the Heat Equation through Integral Transforms*, J. Wiley & Sons, New-York, (2000).
[56] Krapez J.-C., Dohou E., "Thermal quadrupole approaches applied to improve heat transfer computations in multilayered materials with internal heat sources," Int. J. Therm. Sci., 81, pp. 38-51, (2014).
[57] Chen Z.J., Zhang S.-Y. "Thermal depth profiling reconstruction by multilayer thermal quadrupole modeling and particle swarm optimization," Chinese Phys. Lett., 27(2), 026502, (2010).
[58] Krapez J.-C., "Heat diffusion in inhomogeneous graded media: chains of exact solutions by joint Property & Field Darboux Transformations," Int. J. Heat Mass Transf., 99, pp. 485-503, (2016).
[59] Krapez J. C., "Construction of sequences of exact analytical solutions for heat diffusion in graded heterogeneous materials by the Darboux transformation method. Examples for half-space," J. Phys.: Conf. Ser., 745(3), pp. 032059, (2016).
[60] Krapez J. C. "The $\mathrm{sech}(\hat{\xi})$-type profiles: a Swiss-Army knife for exact analytical modeling of thermal diffusion and wave propagation in graded media," Int. J. Thermophysics, 39(7), (2018).
[61] Krapez J. C. "Sequences of exact analytical solutions for plane waves in graded media," J. Mod. Opt., 64(19), pp. 1988-2016, (2017).
[62] Krapez J. C., "Exact analytical modeling of lightwave propagation in planar media with arbitrarily graded index profiles," Proc. Phys. Sim. of Optoelectr. Dev. XXVI (Vol. 10526, p. 1052611). Int. Soc. Opt. Phot., (2018).
[63] Krapez J. C. "Multipurpose S-shaped solvable profiles of the refractive index: application to modeling of antireflection layers and quasicrystals," J. Opt. Soc. Am. A, 35(6), 1039-1052 (2018).
[64] Shvartsburg A.B., "Dispersion of electromagnetic waves in stratified and nonstationnary media (exactly solvable models)," Phys. Uspekhi, 43, pp. 1201-1228, (2000).
[65] Shvartsburg A.B., Maradudin A.A., *Waves in gradient metamaterials*, World Sci. pub., (2013).
[66] Krapez J.-C., *Mesure de l'effusivité thermique - Méthodes photothermiques*, R2959, Techniques de l'Ingénieur. (2007).
[67] Bennett C. A., Patty R. R., "Thermal wave interferometry: a potential application of the photoacoustic effect," Appl. Opt., 21, pp. 49-54, (1982).
[68] Krapez J.-C., "Mesure de l'effusivité thermique par la méthode flash. Application aux matériaux stratifiés," Mémoire de DEA, ECP, (1984).
[69] Balageas D., Krapez J.-C., Cielo P., "Pulsed photothermal modeling of layered materials," J. Appl. Phys., 59, pp. 348-357, (1986).
[70] Martan J., Semmar N., Leborgne C., Lemenn E. Mathias J. "Thermal properties characterization of conductive thin films and surfaces by pulsed lasers," Appl. Surf. Sci., 247, p. 57-63, 2005
[71] Kusiak, A., Martan, J., Battaglia, J. L., Daniel, R. "Using pulsed and modulated photothermal radiometry to measure the thermal conductivity of thin films," Thermoch. Act., 556, 1-5, (2013).
[72] de Hoog F.R., Knight J.H., Stokes A.N., "An improved method for numerical inversion of Laplace transforms," SIAM. J. Sci. Stat. Comp. 3, 357-366, (1982).